

Implications of channel flow analogue models for extrusion of the Higher Himalayan Shear Zone with special reference to the out-of-sequence thrusting

Soumyajit Mukherjee · Hemin A. Koyi ·
Christopher J. Talbot

Received: 2 January 2011 / Accepted: 5 February 2011
© Springer-Verlag 2011

Abstract The Higher Himalayan Shear Zone (HHSZ) contains a ductile top-to-N/NE shear zone—the South Tibetan detachment system-lower (STDS_L) and an out-of-sequence thrust (OOST) as well as a top-to-N/NE normal shear at its northern boundary and ubiquitously distributed compressional top-to-S/SW shear throughout the shear zone. The OOST that was active between 22 Ma and the Holocene, varies in thickness from 50 m to 6 km and in throw from 1.4 to 20 km. Channel flow analogue models of this structural geology were performed in this work. A Newtonian viscous polymer (PDMS) was pushed through a horizontal channel leading to an inclined channel with parallel and upward-diverging boundaries analogous to the HHSZ and allowed to extrude to the free surface. A top-to-N/NE shear zone equivalent to the STDS_U developed spontaneously. This also indirectly connotes an independent flow confined to the southern part of the HHSZ gave rise to the STDS_L. The PDMS originally inside the horizontal channel extruded at a faster rate through the upper part of the inclined channel. The lower boundary of this faster PDMS defined the OOST. The model OOST originated at the corner and reached the vent at positions similar to the natural prototype some time after the channel flow began. The genesis of the OOST seems to be unrelated to any rheologic contrast or climatic effects. Profound variations in the flow parameters along the HHSZ and the extrusive force probably resulted in variations in the

timing, location, thickness and slip parameters of the OOST. Variation in pressure gradient within the model horizontal channel, however, could not be matched with the natural prototype. Channel flow alone presumably did not result in southward propagation of deformation in the Himalaya.

Keywords Channel flow · Higher Himalayan Shear Zone · Detachment · Ductile shearing · Analogue models · Polydimethylsiloxane

Introduction

One of the few longitudinal belts of similar rock types in the Himalaya is the Precambrian and Proterozoic greenschist to amphibolite facies rocks of the ‘Higher Himalayan Shear Zone’ (HHSZ; Mukherjee and Jain 2004; Mukherjee and Koyi 2010a, b and references; Fig. 1). The HHSZ has also been recognized as the ‘Higher Himalayan Crystalline Sequence’, an ‘orogenic channel’, ‘Greater Himalayan Sequence’ and an ‘orogenic wedge’ by different research groups (See Mukherjee and Koyi 2010a, b for review). The justification for designating this part of the Himalaya as a shear zone is that the whole belt had been affected by a ubiquitous ductile top-to-S/SW shear event (the D₂ deformation event of Jain et al. 2002) as revealed by prominent S–C shear fabrics (e.g.; Mukherjee 2007, 2010a, b; Mukherjee and Koyi 2010a,b). The lower boundary of this belt is the Main Central Thrust (Jain and Anand 1988) and the upper boundary is the South Tibetan Detachment System-Upper (STDS_U) (Mukherjee 2007, 2010a; Mukherjee and Koyi 2010a). The rocks of the HHSZ could be one of the following: (i) a high-grade metamorphosed lower tectonic unit of the Lesser Himalaya; (ii) that of an upper unit of

S. Mukherjee (✉)
Department of Earth Sciences, Indian Institute of Technology
Bombay, Powai, Mumbai 400 076, India
e-mail: soumyajitm@gmail.com

H. A. Koyi · C. J. Talbot
Hans Ramberg Tectonic Laboratory, Uppsala University,
752 36 Uppsala, Sweden

Tethyan sediments; (iii) diverse crustal elements mixed with Greater India during a major early Palaeozoic tectonism (review by Robinson et al. 2006).

Several metamorphic and structural aspects of the HHSZ—most notably inverted metamorphism and simultaneity of top-to-N/NE and compressional shearing—have recently almost unanimously been explained by channel flow leading to extrusion of an infrastructure (or the middle crust) (Beaumont et al. 2001; reviews by Burbank 2005; Mukherjee 2005; Grujic 2006; Hodges 2006; Jessup et al. 2006; Yin 2006; Harris 2007; Mukherjee 2007; Dewey 2008; Ashish et al. 2009; Whipple 2009; Mukherjee and Koyi 2010a, b; Owen 2010; also see Harrison 2006; Kohn 2008; Leloup et al. 2010 etc. for counter arguments). Recently, Chambers et al. (2011) postulated that there were several switches in extrusion mode of the Higher Himalaya in the Bhutan Himalaya from channel flow viscous wedge into critical taper frictional wedge and vice versa, where each phase was active for only a few million years. Channel flow leads to minimum shear strain at the centre of the channel and lower values at the boundaries (Mukherjee et al. 2011). The top-to-N/NE shear zone occurring as the uppermost part of the HHSZ has been recognized as the South Tibetan Detachment System, and more recently as South Tibetan Detachment System-Upper by Godin et al. (2006). The STDS_U in the Sutlej and in the Zaskar sections are ductile shear zones (Mukherjee 2007; Mukherjee 2010a, b; Mukherjee and Koyi 2010a). However, the

finding of a second ductile top-to-N/NE shear zone (the South Tibetan Detachment System-Lower—the STDS_L of Godin et al. 2006; review by Mukherjee and Koyi 2010a) and an out-of-sequence thrust (OOST—abbreviated after Morley 1988 and Rowe 2007) in different sections (see reviews by Mukherjee et al. 2009 and Whipple 2009) call for additional interpretation (Fig. 2). As discussed later, the exact timing of the OOST varies along the Himalayan chain. The rationale of taking the OOSTs in different sections as a single thrust active in different time spans is that applied to other major faults. Examples are the MCT_L (15 to 0.7 Ma) and the MCT_U (25 to 14 Ma), and the major normal faults such as the STDS_L (24 to 12 Ma) and the STDS_U (19 to 14 Ma) (Godin et al. 2006).

In two key aspects, therefore, extrusion of the HHSZ via channel flow requires further study. Obvious questions are the following: (i) was the ductile shearing along the two strands at the top-to-N/NE shear zone simultaneous, or sequential? (ii) Could some unforeseen aspect of the extrusion of the HHSZ via channel flow explain the OOST within it? This paper reviews the out-of-sequence thrusting in the Higher Himalayan Shear Zone and uses dynamically scaled analogue models of extrusion by Poiseuille flow and Jeffery-Hamel flow of the HHSZ to address these questions.

Following Mukherjee (2007, 2010c) and Mukherjee and Koyi (2010a, b), we use the term ‘channel flow’ to denote laminar flow of an incompressible Newtonian viscous fluid driven by a pressure gradient between long parallel walls. The

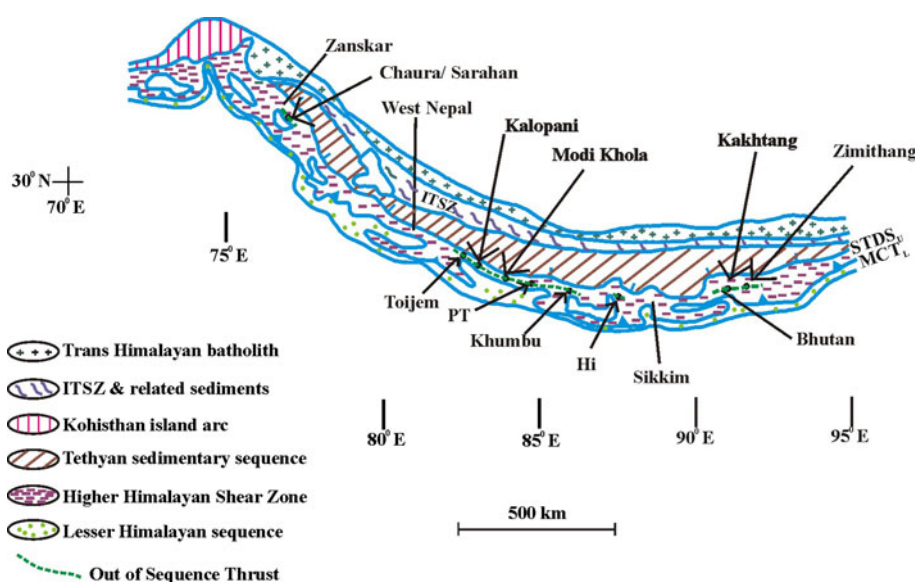


Fig. 1 The out-of sequence thrust (OOST) is delineated passing through spot locations inside the Higher Himalayan Shear Zone (HHSZ) on the map of the Himalayan orogen taken from fig. 1 of Godin et al. (2006). The ‘Greater Himalayan Sequence’ of Godin et al. (2006) is presented here as the HHSZ, and their MCT-zone as the MCT_L. Locations of the OOST were taken from the following references- Chaura/Sarahan: Chambers et al. (2008); Toijem: Carosi

et al. (2007) (However, as per Carosi et al. 2011, the thrust at Toijem is not an OOST); Kalopani: Vannay and Hodges (1996); Modi Khola (Hodges et al. 1996); Physiographic Transition, PT: Wobus et al. (2005); Khumbu: Searle et al. (1995); High Himal Thrust (Hi): Goscombe et al. (2006); Kakhtang: Hollister and Grujic (2006); and Zimithang: Yin et al. (2006)

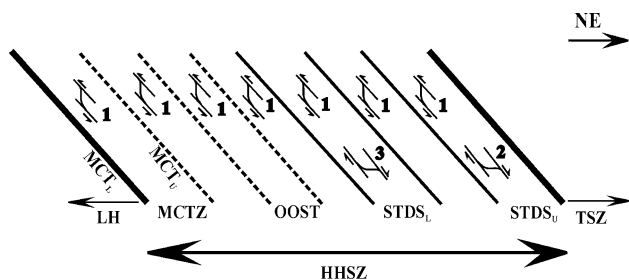


Fig. 2 Summary of the first-order structures from SW to NE across the HHSZ. A top-to-SW sense of shearing ‘1’ occurs everywhere in the HHSZ. Top-to-N/NE shear ‘2’ defines the STDS_U and ‘3’ the STDS_L. No additional fabrics characterize the OOST or the MCTZ; hence, dashes present their boundaries. Symbols: *HHSZ* Higher Himalayan Shear Zone, *TSZ* Tethyan Sedimentary Zone, *STDS_U* South Tibetan Detachment System-Upper; *STDS_L* South Tibetan Detachment System-Lower; *OOST* Out of Sequence Thrust, *LH* Lesser Himalaya; *MCT_L* Main Central Thrust-Lower, *MCT_U* Main Central Thrust-Upper. Neither to scale nor dip

word ‘extrusion’ is used to denote upward movement of rocks that effectively behaved as fluids (similar to Stüwe 2007).

The top-to-N/NE ductile shearing in the South Tibetan detachment system-upper (STDS_U) took place between 19 and 14 Ma and in the South Tibetan detachment system-lower (STDS_L) between 24 and 12 Ma (Godin et al. 2006). However, their activities might not be continuous (Harris 2007). Thus, we do not know whether the ductile top-to-N/NE shear within the STDS_L and the STDS_U (e.g. see Mukherjee 2007, Mukherjee 2010a, b; Mukherjee and Koyi 2010a) were active together during any part of the 19–14 Ma time span. On the other hand, the OOST has been repeatedly linked either with enhanced erosion of its hanging-wall block (review by Whipple 2009) or, more rarely, a channel flow of contrasting lithologies with different rheologies (Carosi et al. 2007). However, neither of these conjectures have been validated by any geodynamic model. Further, the latest numerical channel flow models by the Dalhousie school (e.g. Jamieson et al. 2006) considered the HHSZ to consist of parallel boundaries (Fig. 2). Therefore, Jeffery-Hamel extrusive flow (LeCureux and Burnett 1975 but also others) of the HHSZ through the diverging-upward boundaries deciphered from recent geophysical studies (e.g. as adopted in Fig. 8a in Grujic et al. 1996; see Ashish et al. 2009 for review) has remained unexplored. The dip of the STDS_U at the surface varies between 30° and 60° (Yin 2006’s review) and at depth ranges from 5° to 20° (Ashish et al. 2009’s review) so as to merge with the MCT. A Jeffery-Hamel extrusion can lead to multiple senses of shearing in a single flow. Such complications depend on the Reynolds Number, the pressure gradient that drives the extrusion and the (aperture) angle between the upward diverging boundaries (Fig. 3; LeCureux and Burnett 1975). In such a geometry, the

boundaries of the HHSZ, the STDS_U and the STDS_L would constitute a wedge. The flow would divide with zones of different flow velocities with opposed senses of shear along inflections in the velocity profile. Thus, a possibility remains that the top-to-N/NE shear in the STDS_U and the STDS_L could have been coeval (Fig. 4).

Tectonic framework of the Higher Himalayan Shear Zone

Summary

The following tectono-metamorphic aspects characterize the HHSZ (Fig. 1). (i) Main foliations (i.e. primary shear C-planes) and stretching lineations dip and plunge towards N/NE (Jain and Anand 1988). (ii) Pre-Himalayan D₁- and post-shearing D₃ folds—usually small in scale; ductile synthetic shearing, brittle-ductile extensional boudins, brittle shearing and fracturing are either prior, later or local with respect to the widespread top-to-S/SW ductile shear. Therefore, these deformations are unassociated with extrusion related to ductile shear (Mukherjee and Koyi 2010a, b). (iii) A 1–10-km-thick MCT-Zone (MCTZ) of intense mylonitization which might be a tectonic mélange of Lesser and Higher Himalayan rocks. It is bound by the Main Central Thrust-Lower (MCT_L) and the Main Central Thrust-Upper (MCT_U) (e.g. reviews by Martin et al. 2005 and by Kohn 2008). (iv) Inverted metamorphism above the MCT_L is followed northward by normal sequence

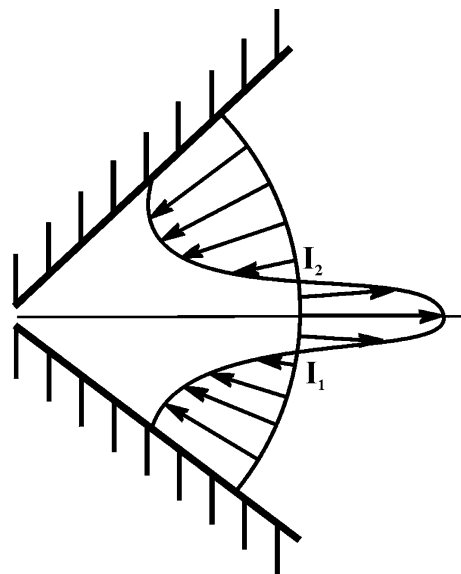


Fig. 3 The curve with two inflection points I_1 and I_2 is a plausible Jeffery-Hamel profile. The circular arc is the inactive marker before the flow (arrows) started. Reproduced from Fig. 11c of Sykes and Reid (1984)

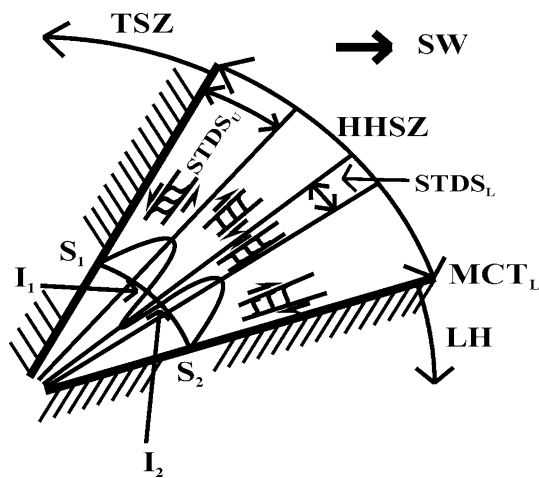


Fig. 4 The HHSZ is defined by north-easterly dipping divergent-upward boundaries. The arc S_1S_2 is a marker before the extrusion. The curve intersecting the marker at the inflection points I_1 and I_2 represents a possible Jeffery-Hamel profile. Had such an extrusion taken place, the $STDS_U$ and the $STDS_L$ would have formed simultaneously with their characteristic shear senses depicted by the S-C fabrics. Symbols defined in caption of Fig. 2

metamorphism (Searle and Rex 1989). (v) A top-to-SW sense of ductile compressional shearing near the MCT_L (Godin et al. 2006), and a zone of ductile top-to-NE sense of shear within the top of the shear zone designated as the $STDS_U$ (Burchfiel et al. 1992). (vi) The presence of a second zone of ductile top-to-N/NE shearing, the $STDS_L$, in some Himalayan sections. These sections include those at Gonto la (Edwards et al. 1996), the Everest massif (Searle 1999; Searle et al. 2003; Law et al. 2004) and the Sutlej section (Mukherjee 2007; Mukherjee and Koyi 2010a). However, the $STDS_L$ is absent in the Alaknanda-, Bhagirathi- (Jain et al. 2002), Dhauliganga and Goriganga sections (observations of the first author) in the Indian Himalaya, and also in the Pakistan Himalaya (Depietro and Pogue 2004). (vii) Simultaneity of top-to-N/NE shear in the $STDS_U$, compressional top-to-S/SW shear in the $MCTZ$ and protracted anatexis and migmatization in the upper part of the shear zone (e.g. Searle et al. 2003). These have been attributed to channel flow that involved 100–200-km horizontal transport of partially molten material (review by Ashish et al. 2009) at a rate of about $5\text{--}6\text{ km Ma}^{-1}$ (see the calculation in Mukherjee and Koyi 2010a). A lithostatic pressure gradient (Grujic et al. 2002) and erosion focused on the HHSZ (Beaumont et al. 2001) have been invoked to drive such channel flow. Partially molten rock materials started flowing as early as 35 Ma along a sub-horizontal channel below Tibet (Lee and Whitehouse 2007) that was linked with the HHSZ. (viii) Compiled mineral cooling ages (Godin et al. 2006) constrain the compressional top-to-SW ductile shearing in the MCT_L to 15–0.7 Ma; and the MCT_U to 25–14 Ma. Similarly, top-to-NE ductile shear in

the $STDS_L$ occurred at 24–12 Ma and in the $STDS_U$ at 19–14 Ma (Godin et al. 2006). This means there is a possibility that the MCT_U , the $STDS_L$ and the $STDS_U$ were active between 19 and 14 Ma; and the MCT_L , the $STDS_L$ and the $STDS_U$ at 14–12 Ma. (ix) A heterogeneous ductile shear regime was dominated by central pure shear and marginal simple shear (Grasemann et al. 2006; Law et al. 2004; review by Exner 2005; Jessup et al. 2006; Carosi et al. 2007; Larson and Godin 2009). (x) The sub-horizontal channel at mid-crustal depth beneath the Tibetan plateau contains 3–7% partially molten rocks (Caldwell et al. 2009). This channel defines a flat that linked to the inclined HHSZ ramp. (xi) Alternately, the tectonic boundaries MCT_L and the $STDS_U$ merge with the Main Himalayan Thrust (MHT) at a depth of ~ 35 km and constitute a wedge (e.g. Fig. 2b of Harris 2006 as deciphered by Grujic et al. 1996). (xii) The occurrence of an out-of-sequence thrust (OOST) in the HHSZ (usually south of the $STDS_L$) in some Himalayan sections (Grujic et al. 1996; Hodges et al. 1996; Vannay and Hodges 1996; Searle 1999; Jain et al. 2000; Grujic et al. 2002; Burbank et al. 2003; Burbank 2005; Wobus et al. 2005; Goscombe et al. 2006; Hollister and Grujic 2006; Yin et al. 2006; Carosi et al. 2007; Harris 2007; Chambers et al. 2008; Wobus et al. 2008; Mukherjee et al. 2009). The next section reviews the OOST within the HHSZ.

Out-of-sequence thrust in the Higher Himalayan Shear Zone—a review

The OOST, a surface-breaking thrust, has been identified within the HHSZ more often from the Nepal- and Bhutan Himalaya (Grujic et al. 1996, 2002; Hodges et al. 1996, 2004; Vannay and Hodges 1996; Searle 1999; Burbank et al. 2003; Wobus et al. 2003, 2005; Wobus 2005; Goscombe et al. 2006; Hollister and Grujic 2006; Carosi et al. 2007; reviews by Burbank 2005; Harris 2007; Mukherjee et al. 2009; Whipple 2009). The OOST lies outside (and below) the $STDS_U$ and the $STDS_L$ and inside the zone of the top-to-SW sense of ductile shearing (Fig. 2). The OOST has been demarcated on the basis of a disparity in extrusion rate in the order of mm per year across it as deduced from geochronological studies. As in the $MCTZ$, no unique structural fabric other than a top-to-S/SW ductile shear of the HHSZ has so far been established in the OOST. This may be due to the parallelism between the shear fabric related to the OOST movement and the pre-existing S-fabrics. Different workers have recognized the OOST at nine main locations along the HHSZ (Fig. 1; Table 1). In the Marsyandi valley in Nepal, near the MCT_U and ~ 23 km south in the adjacent valleys, a high rate of exhumation in the Pliocene–Pleistocene has been recorded across a 3–5-km-thick (Wobus et al. 2006a)

tectonic zone called the ‘physiographic transition’ by Burbank et al. (2003), Burbank (2005), Wobus et al. (2005), Harris (2007, review) and possibly also by Wobus et al. (2008) (‘physiographic transition-2’ by Hodges et al. 2004 and Wobus et al. 2006a). The physiographic transition has also been considered as the reactivated MCT in a new location (Wobus et al. 2006a, b). These workers considered the MCT_U as the lower boundary of the HHSZ. Taking the MCT_L (that passes at least 30 km north-east of Kathmandu) as the lower boundary of the HHSZ, the physiographic transition comes inside the shear zone in a position similar to that of the OOST at other sections. Thus, the physiographic transition and the OOST are likely to be a single element (Fig. 1). The OOST is quite pervasive beneath Kakhtang and either initiates where the MCTZ branches out from the MHT at a depth of ≥ 30 km, or extends for 200–300 km northward beneath the Tibetan plateau (Fig. 5—simplified from Grujic et al. 2002; Hollister and Grujic 2006—especially their fig. 5). Five strands of physiographic transitions have also been reported from the HHSZ in Bhutan. Two of them—the PT2a and the PT2b—are ~ 10 km thick (Wobus et al. 2003)—and may indicate an out-of-sequence blind thrust (Tobgay and Hurtado JM Jr 2004; Tobgay 2005). Similarly, the OOST has been interpreted as a blind thrust south of the MCT (= MCT_U of Godin et al. 2006) in the Kumaun Himalaya (Paul et al. 2010).

Recently Carosi et al. (2010) deciphered that activity of the so-called OOST at Toijem peaked at around 26 Ma and continued until 17 Ma. Thus, these authors considered the shear zone at Toijem to be one of the oldest extrusion zones in the HHSZ. If this is so, the shear zone at Toijem cannot be equated with OOST. We therefore take into consideration only the position of the Toijem Shear Zone (in Figs. 1, 6) bearing in mind that it need not be an OOST and reconsider it later in the light of our model results (Fig. 14 for example).

Geochronological studies on the OOST indicate different phases of activity from section to section (Table 1). The OOST is still active only in the Marsyandi valley, Nepal Himalaya. The timing of channel flow in different sections of the HHSZ is conventionally equated with the common span of compressional shearing in the MCTZ and ductile top-to-N/NE shearing in either the $STDS_U$ or the $STDS_L$. In sections where the timings are known for both the top-to-N/NE and the top-to-S/SW compressional shear, the channel flow and extrusion is usually found to precede activity in the OOST. For example, following Hodges et al.’s (1996) geochronological data in Modi Khola, the possible initiation of channel flow was around 22.5 Ma. In Kakhtang, channel flow was active from 22 to 13 Ma (Hollister and Grujic 2006). The activity of the MCTZ in the Marsyandi section occurred between 22 and 16 Ma (data from Coleman 1998; Catlos et al. 2001). Therefore,

even though we have no data on the timing of top-to-N/NE ductile shear in the Marsyandi section, it can be safely inferred that there was no channel flow before 16 Ma. The timing of activation of the OOST at Kalopani and Modi Khola has been constrained to between 22 and 15 Ma (Vannay and Hodges 1996; Godin et al. 2001). This means that the known timing of the out-of-sequence thrusting in the HHSZ along the Himalayan trend ranges from 22 Ma to the Holocene. Notice that there is an overlap of this timing of the OOST with those compiled by Godin et al. (2006) for the MCT_U , the MCT_L , the $STDS_U$ and the $STDS_L$. More specifically, activity on the OOST at Kakhtang was simultaneous with the ductile top-to-N/NE shear in the $STDS_U$ between 11 to 10 Ma (Grujic et al. 2002; Hollister and Grujic 2006). On the other hand, the High Himal Thrust and the $STDS_U$ were active together between 22 to 11 Ma (Goscombe et al. 2006).

The OOST, at Kakhtang (Grujic et al. 2002), Toijem (as per Carosi et al. 2007 but that contradicted by Carosi et al. 2010) and Chaura (Jain et al. 2000), is a ductile shear zone with a top-to-SW sense of shear affecting high-grade minerals with a later imprint of brittle shear of the same sense at Chaura (Jain et al. 2000). The dominant lithologies in the hanging wall side of the OOST are migmatites and leucogranites in several sections: for example, at Khumbu (Searle 1999), Zimithang (Yin et al. 2006), Toijem (Carosi et al. 2007; Carosi et al. 2010) and Kakhtang (Grujic et al. 2002; Hollister and Grujic 2006). The leucogranite might be indicative of decompression due to shear on the OOST (Carosi et al. 2010). However, the footwall contains leucogranites and migmatites, e.g. at Modi Khola (Hodges et al. 1996), that for the High Himal Thrust (Goscombe et al. 2006) and at Sarahan (Chambers et al. 2008). The High Himal Thrust dips 20–40° to the E/ENE/NW, and exhibits mylonitization of garnet, sillimanite and feldspar bearing rocks, northward plunging stretching lineations, shear bands, and a very high strain ratio (R) of between 30 and 45 (Goscombe et al. 2006). In contrast to all other places, the OOST in Nepal (where it is recognized as High Himal Thrust) underwent a late phase of extensional faulting (Goscombe et al. 2006; also referred to in Imayama et al. 2010).

The thickness of the HHSZ varies from section to section (reviews by Mukherjee 2007; Mukherjee and Koyi 2010a). The position of the OOST inside the HHSZ can be represented by the ratio of distances between the MCT_L and the OOST to between the OOST and the $STDS_U$ (Table, 1; Fig. 6). The ratio is found to vary in different sections. This may be due to a variation in the thickness of the HHSZ from a minimum of 2 km in the Nepalese Himalaya (Godin et al. 2006) to a maximum of 50 km around Zanskar (Stephenson et al. 2000).

Along the Himalayan chain, the OOST varies significantly in its time of activity, location in the HHSZ,

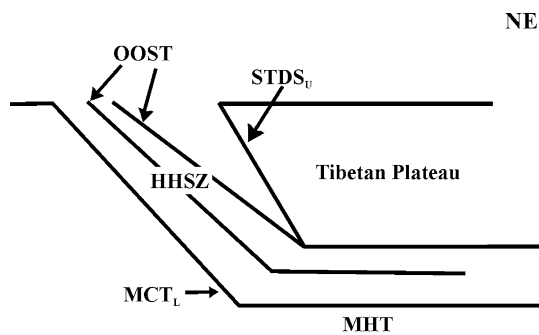


Fig. 5 Schematic representation of possible occurrences of the OOST (from Grujic et al. 2002; Hollister and Grujic 2006). The OOST either originates from where the $STDS_U$ joins the sub-horizontal channel or continues through the latter. Symbols defined in caption of Fig. 2. Neither to scale nor dip

thickness and its amount of displacement (Table 1). For example, taking the optimum values of activation of the OOST as 22.5 Ma at Modi Khola (Hodges et al. 1996) and the Holocene in the Marsyandi section (Burbank 2005; review by Harris 2007) that are merely ~ 83 km apart, the maximum variation in the timing of the OOST is ~ 22.5 Ma. Taking the relative location of the OOST inside the HHSZ as the ratio of distance between the MCT_L to the OOST and that between the OOST and the $STDS_U$ varies within the range of 1:0.25 to 1:1.57 (Fig. 6).

Channel flow analogue models

Model design and material

A ‘channel flow box’ was designed and built in plexiglass at the Hans Ramberg Tectonic Laboratory at Uppsala University. The box consists of a piston, a base plate, a

front plate, two side plates, two hanging-wall wedges and two foot-wall wedges (Fig. 7). Wedges with different slopes were prepared. When the plates and the wedges are installed, the box consists of a horizontal (flat) channel venting through an inclined or ramp channel. The box can be dismantled into two mirror-image halves. Polydimethylsiloxane (PDMS), a transparent incompressible Newtonian viscous polymer with a density of 0.95 gm cm^{-3} and a viscosity of 10^5 Pa s (reviews by Koyi 1991; Talbot and Aftabi 2004), was used as the model material. We used PDMS because (i) its rheology is well known; (ii) it is widely used in various other analogue models (Talbot and Aftabi 2004; Exner 2005); and (iii) its transparent nature allows monitoring the deformation of grids inside it. Godin et al. (2011) also used PDMS as an analogue for mid-crustal partial melt beneath the Himalaya. A single model material was used in our experiments since (i) it was difficult to place two model materials inside the channel flow box; and more importantly (ii) if two materials were used—one for stiff rocks and the other with a lower viscosity to represent the partially molten rock in the prototype, it would have been impossible to prove that this rheological contrast is not a necessary factor for generating the OOST (discussed latter).

In different experiments (the 8th column in Table 2), masses of 634 to 1033 gm of PDMS were inserted within the two halves of the channel flow box. These were then left undisturbed for a few days to allow the air bubbles to rise and vent to the temporary free surfaces. For each experiment, two partially photocopied grids of unbaked carbon on transparent sheets were imprinted on the PDMS along what was to become the vertical mid-plane. After printing one grid in the horizontal channel and the other in the inclined channel, the two halves of the channel flow box were rapidly screwed together (Fig. 8a). For

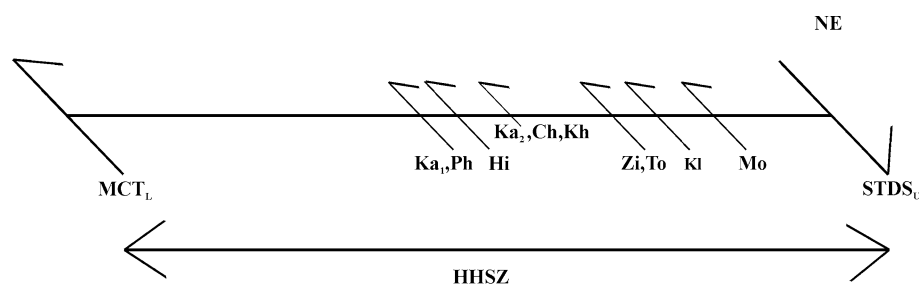


Fig. 6 The relative locations of the OOST— Ka_1 , Ph, Ka_2 , Ch, Kh, Hi, Zi To, Kl and Mo—as noted in different sections of the HHSZ. Topography is neglected. The ratio of distance between the MCT_L to the OOST to that from the OOST to the $STDS_U$ are maintained constant. The Ka_2 coincides with the Ch. The $STDS_U$ shows dominantly a top-to-NE sense of shearing, whereas it shows a top-to-SW shear sense at other locations. Symbols (and references from which ratios were calculated)— MCT_L Main Central Thrust-Lower, Ka_1 Kakhtang Thrust (Grujic et al. 2002), Ka_2 Kakhtang Thrust

(Hollister and Grujic 2006), Ph Physiographic Transition (Harrison et al. 1997, Wobus et al. 2005), Hi High Himal Thrust (HHT), Ch Chaura Thrust (Jain et al. 2000, Chambers et al. 2008), Kh Khumbu Thrust (Searle 1999); Hi: Higher Himal Thrust (Goscombe et al. 2006), Zi Zimithang Thrust (Yin et al. 2006), To Toijem Shear Zone (Carosi et al. 2007; however, as per Carosi et al. 2010, the thrust at Toijem is not an OOST), Kl Kalopani Shear Zone (Vannay and Hodges 1996), Mo Modi Khola Shear Zone (Hodges et al. 1996). Other symbols defined in caption of Fig. 2

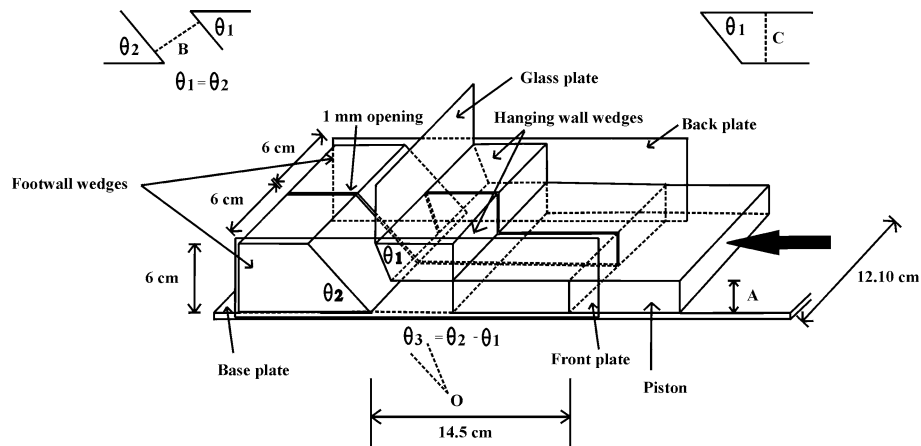


Fig. 7 The channel flow box consisting of an inclined channel analogous to the Higher Himalayan Shear Zone (HHSZ) linked to a horizontal channel. A pair of hanging wall and footwall wedges constitutes the inclined channel. For a diverging-upward inclined channel ($\theta_1 > \theta_2$), the aperture angle is $\theta_3 = \theta_1 - \theta_2$. Dimension ‘A’—thicknesses of the horizontal channel; ‘B’—that of the HHSZ;

‘C’—the depth at which the inclined channel meets the horizontal channel = 3.5 cm in models. Along the vertical mid-plane—the ‘1 mm opening’ between the two halves of the wedges, grids were imprinted on the PDMS. A rectangular piston pushed the PDMS filling the horizontal channel to the left. A ‘glass plate’ in some experiments restricted the flow of the extruded PDMS. Not to scale

experiments with parallel inclined boundaries (experiment numbers 1, 5, 7 to 10 in Table 2; Figs. 8a, 11a, 11c), the grids were of equally spaced sets of perpendicular lines. For experiments with diverging-upward inclined channels (experiment numbers 2, 3, 4, 6 in Table 2; Figs. 8d, 10a, 10c, 11d), the grids consisted of arcs and radial markers. Grid lines acted as passive markers in all the experiments. PDMS being an incompressible fluid, these experiments implicitly neglected any kinematic dilatancy due to partial melting (Grasemann et al. 2006) during extrusion of the HHSZ related to channel flow. Using PDMS also precluded modelling the brittle behaviour of rocks at depths of ≤ 8 km in the natural prototype. As extruding rocks reaches shallower levels, their temperature is expected to fall and their viscosity to rise. Neither the present models nor any other published (analogue) models can take into account this change (e.g. Ramberg 1981; Koyi 1991; Koyi 1997; Talbot and Aftabi 2004; Mukherjee 2010c; Mukherjee et al. 2010; Mukherjee and Mulchrone 2011). The second important constraint worth mentioning is that since controlled removal of the extruded PDMS was impractical, the extruding PDMS was allowed to gravity spread without any erosion.

Similarity factors

For a one-to-one compatibility, the analogue models must be geometrically, dynamically and kinematically similar to the natural prototype (e.g. Ramberg 1981; Koyi 1997). The dips of the boundaries of the inclined channel that acted as the model HHSZ were taken as 30° , 40° and 60° following those construed by Vannay and Grasemann (2001),

Robinson et al. (2003), Jamieson et al. (2004) and Yin (2006). The boundaries were parallel and diverging-upward in different experiments. Reasonable geometric similarity between the analogue models and the HHSZ in the natural prototype was achieved by choosing the thickness of the horizontal channel (‘B’ in Fig. 7) to be 15–50 km (from Jamieson et al. 2004; and Acharya and Ray 1977) and the depth (‘C’ in Fig. 7) of the upper boundary of the horizontal channel to be 35 km (average value from Fig. 8b of Hauck et al. 1998). The thickness of the HHSZ has been reported to vary from 2 to 50 km (the ‘A’ parameter in Fig. 7; see Godin et al. 2006 for the minimum and Stephenson et al. 2000 for the maximum values). If we choose parameter ‘B’ suitable for the laboratory equipment as 15–50 mm and the ‘C’ as 35 mm, it would be difficult to document deformation patterns in a geometrically similar inclined channel where the lower practical limit of the ‘A’ parameter becomes 2 mm. For this reason, we chose the ‘A’ parameter as 1.25–5 cm. Different experiments involved three combinations of thicknesses of the inclined—and the horizontal channels: (i) they were of equal thickness, (ii) the inclined channel was twice the thickness of the horizontal channel, and (iii) the horizontal channel was twice the thickness of the inclined channel. The same thickness relations of the two channels were also considered by Beaumont et al. (2004) (also see Fig. 2 of Langille et al. 2010). As both the natural prototype and the analogue models maintained Reynolds Numbers much less than unity (Eq. 3 onwards in the “Appendix”), they are dynamically similar (as per Schlichting and Gersten 1999). However, the boundaries of the model channel were static whereas in the natural situation, these boundaries migrated southward with time (Jamieson

Table 2 Specifications and results of analogue models

Exp no.		Experiment specifications										Results							
		Channel flow box configuration										From horizontal channel				From inclined channel			
		θ_1	θ_2	θ_3	A (cm)	B (cm)	Glass plate at margin of upper inclined wall	PDMS mass inside channel flow box (gm)	Exp continued till (min)	Pressure gradient measured till (min)	Gear Driving the piston	Piston velocity (mm per 10 min)	Pressure gradient versus time (modify?)	Simulated extensional shear zone	Model OOST crops to surface at (min)	Ratio of distance between MCT _L to OOST and that between OOST to STD _{S,U}			
											a	b	Corr. Coeff. (r)						
1	40	40	0	2.50	2.50	Not used	634	231	214	0.3	3.13	44	-28	0.98	STDS _U	215	1:1.57		
2	40	30	10	2.50	D	Not used	728.4	202	104	0.3	3.12	0.07	2.1	0.998	STDS _U	200	1:0.93		
3	60	30	30	2.50	D	Not used	771.3	353	98	0.3	0.29	0.08	1.9	0.999	STDS _U	204	1:1.15		
4	60	30	30	2.50	D	Not used	771.3	250	54	0.6	6.02	0.16	18.5	0.99	STDS _U	100	1:0.46		
5	40	40	0	2.50	2.50	Not used	634	252	43	0.6	8.37	0.14	15.2	0.983	STDS _U	40	1:0.25		
6	40	30	10	2.50	D	Used	728.4	423	126	0.3	2.82	0.06	19.8	0.976	STDS _U	270	1:0.92		
7	30	30	0	2.50	5.0	Used	1032.7	484	38	0.3	2.6	0.08	45.6	0.967	STDS _U	373	1:0.28		
8	30	30	0	2.50	5.0	Not used	1032.7	48	42	0.6	5.74	2	28.1	0.996	STDS _U	NM	NM		
9	30	30	0	2.50	1.25	Not used	519.7	55	49	0.6	6.08	0.18	22.71	0.99	STDS _U	NM	NM		
10	30	30	0	2.50	1.25	Not used	519.7	80	79	0.3	3.47	0.11	36.77	0.997	STDS _U	NM	NM		

The parameters ' θ_1 ', ' θ_2 ', ' θ_3 ', 'A' and 'B' are defined in Fig. 8. The parameters 'a' and 'b' occur in Eq. 2 in the "Appendix". In experiment 6, a pulsed flow was induced. The piston was pushed between: 0–62 min, 126–182 min, 243–303 min, and 363–423 min. The piston was stopped between: 62–126 min, 182–243 min and 303–363 min
GD gently diverging-up inclined channel, *SD* strongly diverging-up inclined channel, *D* diverging, *P* parallel wall inclined channel, *NM* not measured

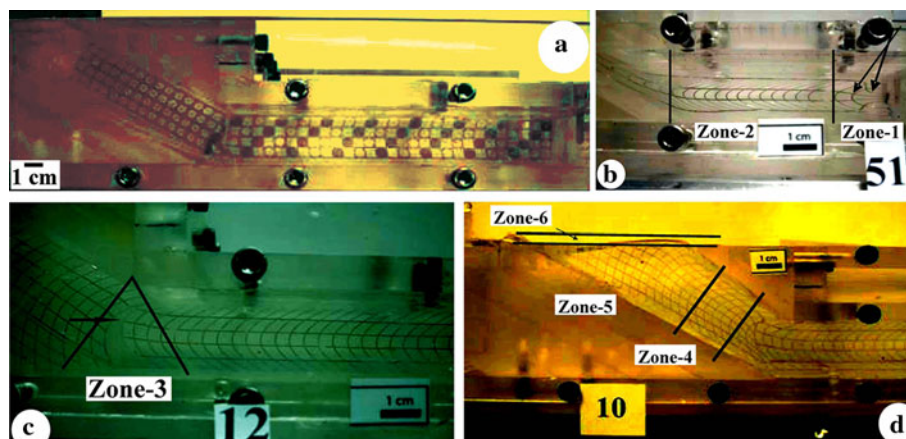


Fig. 8 **a** The channel flow box full of PDMS, with grids imprinted along its vertical mid-plane before the onset of deformation. The smallest squares in the grids are 5×5 mm. **b** Pushing the piston in the horizontal channel developed flow zones 1 and -2. In zone 1, grids pinched (*arrow*) into a tilted pitcher-shape. Zone 2 was defined by congruent parabolas. Experiment 3. Photo 15. Time: 64 min. **c** Zone 3 was defined at the corner where the parabolic velocity profile in the horizontal channel entered the inclined channel. Grid lines initially horizontal became inclined as they entered the inclined channel

(*arrow*). The vertices of the profiles shifted towards the upper boundary of the inclined channel. Experiment 7. Photo 12. Time: 20 min 32 s. **d** Flow zone 4 was defined by parabolic velocity profiles with vertices along the middle of the inclined channel. The flow zone 5 was near the opening of the inclined channel. Here, the velocity profiles were somewhat rounded with vertices shifted near the upper inclined boundary. Flow zone 6 was the PDMS extruded above the horizontal vent. Experiment 2. Photo 10. Time: 35 min

et al. 2004). The models and their prototypes therefore differed kinematically in a Eulerian reference frame fixed to India, but were kinematically similar in Lagrangian coordinates fixed on the channel boundaries. We assume the acceleration due to gravity during the time of deformation of the prototype HHSZ to be the same as at present as usual in all modelling of tectonics on Earth—analogue or numerical (e.g. Ramberg 1981; Koyi 1991; Koyi 1997; Beaumont et al. 2001; Talbot and Aftabi 2004; Mukherjee et al. 2010; Mukherjee and Mulchrone 2011).

Results and discussions

Ten experiments were performed in the channel flow box with the top and bottom boundaries of the inclined channel parallel in some models and diverging-upward in others. PDMS was extruded through the inclined channel by using a low-g geared step motor to drive the piston along the horizontal channel at a constant rate that varied from 0.25 to 6 mm per 10 min in different experiments performed over 1 to 8 h (the 9th column in Table 2). We appreciate that the model drive is a great simplification of Himalayan tectonics where channel flow appears to be driven by either a pressure gradient created by the over-thickened Tibetan crust (Grujic et al. 2002), a high rate of erosion induced by excessive monsoonal rainfall (Beaumont et al. 2001), or both. However, the experiments were not intended to test the driving mechanism. Instead, they were designed to study how the parabolic velocity profiles along the

horizontal channel adapted to extrusion through an inclined HHSZ with different geometries. The parabolic profile is intrinsically related to the flow mechanism and is independent of friction at the two boundaries (e.g. Pai 1956; Schlichting and Gersten 1999). Secondly, over the past 10,000 years, shortening across the MHT at ~ 2 cm year⁻¹ could account for all of the India-Eurasia convergence (Hodges et al. 2004). Most plausibly, the deformation (and any slip) in the HHSZ during this period, as modelled here, was entirely due to channel flow.

The transparency of the PDMS allowed monitoring of how the initial marker grids (e.g. Fig. 8a) deformed with time. In experiments 7 and 8, a vertical glass plate was

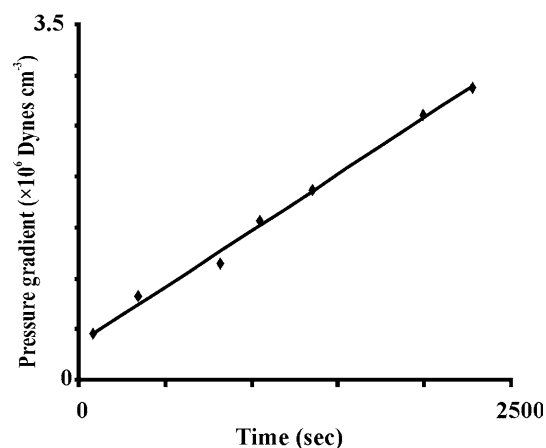


Fig. 9 Plots of pressure gradient versus time as calculated from zone 2. Experiment 10

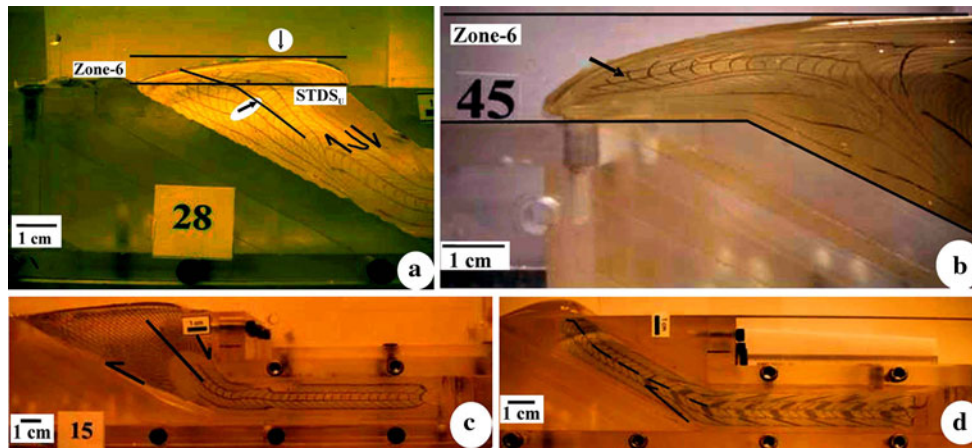


Fig. 10 **a** Zone-6 thickened (arrow inside circle) as time passed. The round-hinge folded markers in zone 6 were non-parallel to the extrusion profile. The inclined channel was divided into a zone of compressional top-to-S/SW shear at left and a top-to-N/NE shear at right across a line (arrow inside ellipse). An intrafolial fold developed at the contact between grids that were initially within the inclined channel and that within the horizontal channel. Markers diverged upwards in the inclined channel (arrow within white elliptical background). Experiment 2. Photo 28. Time: 111 min. **b** The PDMS in zone 6 underwent gravitational spreading preferentially towards the lower boundary of the inclined channel where the grids developed

upright and reclined folds (arrow). Experiment 7. Photo 45. Time: 7 h 15 min. **c** Pushing the piston in the horizontal channel, the PDMS extrudes from the inclined channel. The extrusion in the initial stage is shown. A line in the inclined channel demarcates the zones of compressional top-to-S/SW shearing at left from that of top-to-N/NE shear at right. Experiment 4. Photo 15. Time: 64 min. **d** An out-of-sequence blind thrust formed at zone 3 inside the zone of compressional top-to-S/SW shear. The curved dashed line separates the zone of compressional top-to-S/SW shearing at left from that of top-to-N/NE shear at right. Experiment 1. Photo 12. Time: 90 min

fixed at the down-dip side of the extrusion vent so that the extruded PDMS gravity spread preferentially towards the up-dip direction of the model HSHZ. The rationale for adding this plate was that nappe movement of the HHSZ, presumably a result of its protracted extrusion, took place exclusively towards the up-dip (south or south-west) direction of the MCT_L (Thakur 1992; Fig. 2b of Vannay and Grasemann 2001). In one of the models (experiment 6), the piston was pushed intermittently to simulate the pulsed channel flow around 45 and 25 Ma throughout the HHSZ proposed by Jain et al. (2005) and Singh et al. (2005) based on SHRIMP U–Pb dating of zircons from Garhwal Himalaya.

By the time the piston moved more than about half the length of the horizontal channel, the imprinted markers in the PDMS were too blurred and distorted to track. For this reason, it was usually possible to only measure the pressure gradient (Eq. 1 onwards in the “Appendix”) for the first half of most experiments (Table 2). Observations common to all the models in the first half of their duration, including those with parallel and diverging-upward inclined channels, were as follows.

(1) Six flow domains were visually distinguishable in the complete channel. From the PDMS in contact with the piston towards the vent at the top of the inclined channel, these domains are: (i) Zone 1: markers that were initially vertical became rounded and resembled tilted pitchers (Figs. 8a, 12a). These profiles were related to the advancing piston and, therefore, are not expected in nature. (ii)

Zone 2: in the horizontal channel, the vertical markers were deformed into congruent parabolas recording channel—or Poiseuille flow (Figs. 8b, 12a). (iii) Zone 3: the corner joining the horizontal and the inclined channel (Figs. 8c, 12a). After the symmetric parabolic markers in zone 2 entered this zone, they become asymmetric as their vertices shifted towards the upper boundary of the inclined channel. (iv) Zone 4: low in the inclined channel, markers that were perpendicular to the inclined boundaries assumed parabolic profiles with vertices equidistant from the boundaries (Figs. 8d, 12a). (v) Zone 5: in the inclined channel, markers initially perpendicular to the boundaries became parabolic but somewhat more rounded (Figs. 8d, 12a). And (vi) Zone 6: The PDMS extruded out of the vent defines this zone. The extrusion profile was parabolic with its vertex located closer to the upper boundary of the inclined channel in the early stages (Figs. 8d, 12a). As the piston advanced along the horizontal channel, zones 1 to 5 were pushed proximally through the box. Given the Newtonian rheology of the PDMS, the pulsed extrusion resulting from experiment 6 only differed from its steady equivalent in the prolongation of the gravity spreading of the PDMS in zone 6; the geometries of the other five flow zones inside the horizontal—and the inclined channel were the same.

(2) In zone 2, the parabolic velocity profiles became more and more tapered as the piston advanced. The plane Poiseuille flow/channel flow developed a progressively increasing pressure gradient (Eq. 2 in the “Appendix”) as predicted by Massey (1975). This was also in accordance

with a variety of Poiseuille flow described by Pai (1956), where the pressure gradient is time dependent. In the analogue models, the pressure gradient in zone-2 increased linearly with time (Fig. 9; Eq. 2 in the “Appendix”, Table 2). It is, however, not known whether or not the pressure gradient that drove the prototype channel flow resulting in the extrusion of the HHSZ was time dependent. This is because only single magnitudes of pressure gradient are known from some sections of the HHSZ. An example is the estimate of $1.0\text{--}2.0\text{ kb km}^{-1}$ in the Bhutan Himalaya (see Mukherjee and Koyi 2010a for review).

(3) In zones 4 and 5, markers initially parallel to the inclined boundaries diverged upward (Fig. 10a).

(4) In zone 4, an intrafolial fold formed near the contact between the different grids that were initially in the horizontal and the inclined channel. The shear sense indicated by this single fold was given by the top-to-NE sense of ductile shear regime where it formed (Fig. 10a). Interestingly, such folds were documented from the $STDS_U$ and the $STDS_L$ in field studies in the Sutlej section (Mukherjee and Koyi 2010a; unpublished photographs by the first author). In a few of our experiments (not shown), the broad geometry of the flow profiles in different zones remained the same however much of the extruded PDMS was removed in an unconstrained way.

(5) In zone 6, markers initially parallel to the boundaries of the inclined channel became round-hinge folds that were discordant to the parabolic profile of the extruded PDMS

(Fig. 10b). As time progressed in each experiment, the extruded PDMS in zone 6 underwent gravity spreading and lost its parabolic shape.

(6) A single ductile top-to-N/NE shear zone formed near the upper boundary of the inclined channel within zones 4 and 5 (Figs. 10c, d, 12a). This top-to-N/NE shear was contemporaneous with the compressional shear that occurred near the lower boundary of the inclined channel. The shear sense was deduced from deformed markers that were initially perpendicular to the boundaries of the inclined channel. From its appearance within the upper part of the inclined channel, the top-to-N/NE shear zone was comparable with the $STDS_U$ of the HHSZ. As the flow profiles in zone 4 was parabolic and rounded in zone-5, no second top-to-NE shear zone formed simultaneously inside the inclined model channel to simulate the $STDS_L$.

We, therefore, infer that a pressure gradient induced flow must have operated in two pulses to produce the two strands of the top-to-N/NE shear zone represented by the $STDS_U$ and the $STDS_L$. As in our models, one of the pulses was activated from the MCTZ up to the top boundary of the HHSZ giving rise to the $STDS_U$. Where the $STDS_L$ exists in a few sections, the other pulse would have occupied the lower part of the HHSZ—from the MCTZ up to the top of the now $STDS_L$ as the two boundaries. Considering the compiled data of activation of the $STDS_U$ and the $STDS_L$ along the Himalayan trend as presented by Godin et al. (2006), it can therefore be said that both the $STDS_U$ and the

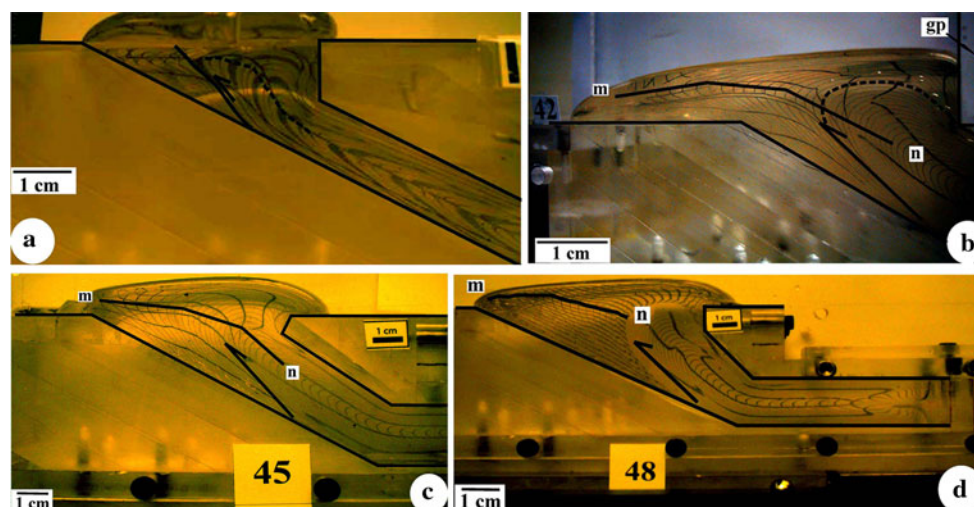


Fig. 11 **a** The out-of-sequence thrust reached the vent within the compressional top-to-S/SW shear regime late in the experiment. The thrust dipped towards the upper boundary of the inclined channel and defined a wedge with the lower boundary. Experiment 1. Photo 22. Time: 215 min. **b** Prolonging the experiment led to gravitational spreading of the extruded PDMS together with the out-of-sequence thrust (arrow) reaching the vent within the zone of compressional top-to-SW shear. The broken line is the outer limit of the PDMS that was initially within the horizontal channel. Line ‘mn’ separates the zone

of compressional top-to-SW shear at left from that of top-to-N/NE shear at right. The glass plate ‘gp’ prevented gravitational spreading of the extrusion to the right. Experiment 7. Photo 42. Time: 6 h 13 min. **c, d** Line ‘mn’ separates the zone of compressional top-to-SW shear at left from the zone of a top-to-NE shear at right. The out-of-sequence thrust developed within the compressional top-to-SW shear zone. **c** Experiment 2. Photo 45. Time: 3 h 5 min. **d** Experiment 3. Photo 48. Time: 3 h 40 min

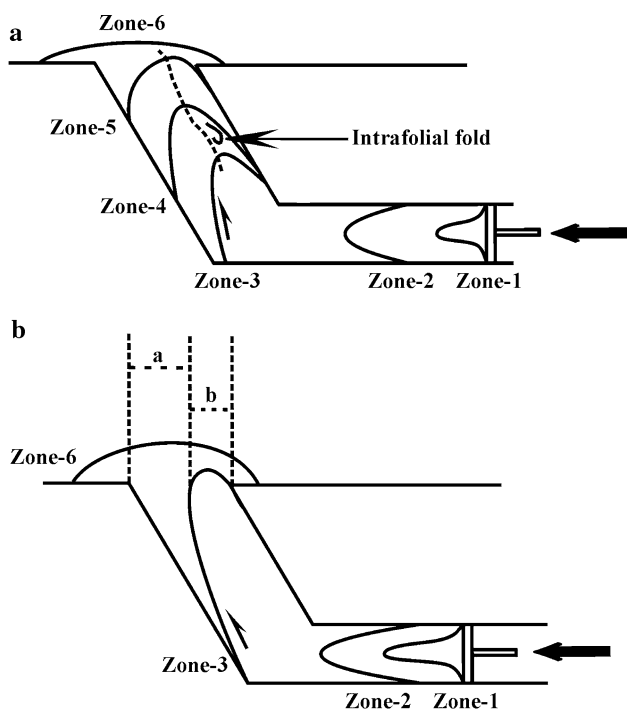


Fig. 12 Development and evolution of flow profiles in the channel flow box. **a** Zone 1: at the contact with the piston, tilted pitcher like velocity profile; zone 2: parabolic profiles; zone 3: profile formed at the corner; zone 4: parabolic profiles; zone 5: rounded profiles; and zone 6: the extrusion profile. Half arrow in zone 3: an out-of-sequence thrust (OOST). *Solid arrow* piston push. *Dashed line* boundary between the zone of a top-to-N/NE shear at right and that of compressional top-to-S/SW shear at left. An intrafolial fold formed between zones 3 and 4. **b** Further piston push led to the OOST reaching the vent. The parabola in zone 2 became more tapered as the extruded PDMS accumulated. The ratio a:b has been measured for different experiments and presented in Table 1 and in Fig. 14. Neither to scale nor dip

STDS_L did not simultaneously activate between 19 and 14 Ma or in any segment of this time span. In our analogue models, a more specific time relation between these two pulses remained indeterminate.

In some Himalayan sections, either the STDS_L is absent or we do not yet know the timing of activity of the STDS_U or the STDS_L. For example, only the STDS_L is known to

have been activate between 23 and 17 Ma in the Sutlej section (Vannay et al. 2004), but the timing of the STDS_U is not known. In specific sections, however, where the times of activity of these two top-to-N/NE shear zones are known, their simultaneity should differ from the average timing of 19–14 Ma for the entire Himalayan trend. For example, Godin et al. (2006) compiled the possible spans of activities of the STDS_U in the Everest Himalaya as 16 Ma, <16 Ma, 17 Ma and 22–19 Ma, and the STDS_L as 21 Ma, 18–17 Ma and <20.5 Ma.

(7) As the piston advanced, the PDMS that began inside the horizontal channel moved up through the inclined channel but preferentially through its upper portion as zone 3 (Figs. 10c, d; 11a–d, 12a, b). The velocity of the PDMS in the upper portion of the inclined channel was greater than that in the lower portion occupied by PDMS that was originally in the lower channel. A similar relationship is also deciphered from the specific geometry of the prolonged profile of the zone-3 in the middle to the late stage of experiments. In effect, the lower boundary of the fast moving PDMS now inside the inclined channel acted as a ductile thrust with a hanging wall that extruded faster than its footwall. However, the PDMS, originally inside the inclined channel, that extruded ahead of zone 3 still occupied the whole of the inclined channel so that the differential flow gradient did not reach the surface. In other words, (i) extrusion within the inclined channel self-adjusted from flow occupying the complete channel into a faster flow along the upper wall, and (ii) the ductile thrust initiated in zone 3, was not immediately manifest at the surface. It took time for the new flow profile picked up at the corner to reach the vent. Having formed in zone 3 with a dip parallel to the top of the inclined channel, this blind thrust was carried upward through zone 4 and 5 and finally cropped out closer to the lower boundary of the inclined channel. The thrust was carried to the vent an hour or more after the channel flow/Jeffery-Hamel flow initiated in PDMS entering zone 3.

As in the natural prototype, this thrust remained within the ductile top-to-S/SW shear regime from its formation up

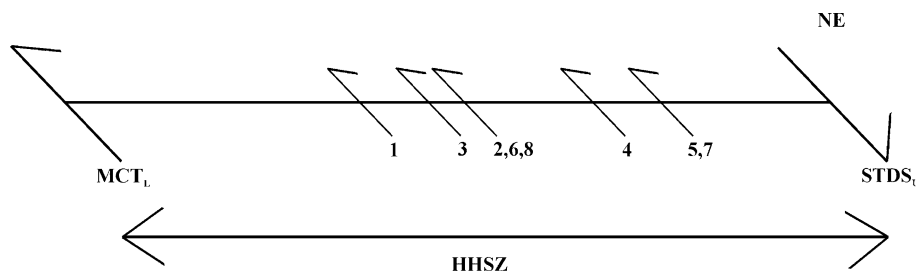


Fig. 13 The location of the OOST simulated in analogue models is schematically represented in the HHSZ. Topography is neglected. Numbers stand for the OOSTs in respective experiments. The ratio of

distance between the MCT_L to the OOST and that between the OOST and the STDS_U are presented in Table 1. Symbols explained in caption of Fig. 2

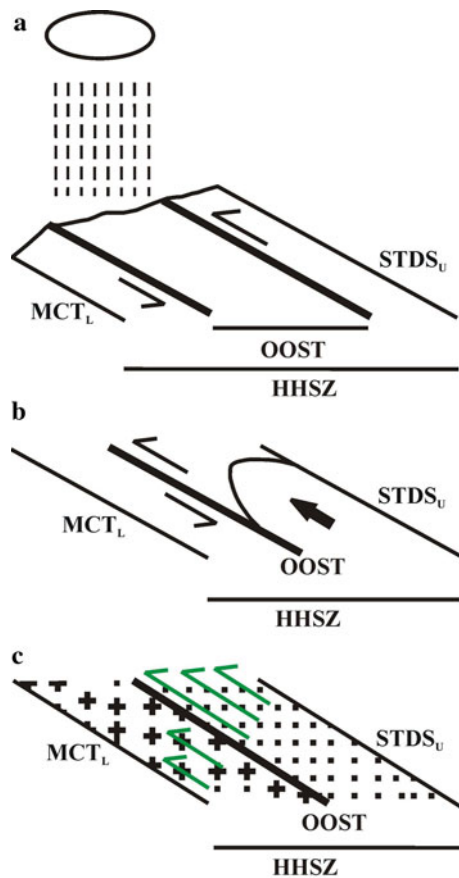


Fig. 14 Hypotheses for the genesis of the OOST within in the HHSZ. **a** Excessive rainfall and subsequently a high rate of erosion inside the HHSZ gave rise to OOST. Simplified and modified from Harris (2007). **b** Channel flow within the HHSZ was restricted to above the OOST. From Hollister and Grujic (2006). **c** Extrusion of the HHSZ having two rheologies. The OOST lies at the interface between the two rock types. Taken from Carosi et al. (2007). Symbols defined in caption of Fig. 2

to its appearance at the vent. In models that developed such ductile thrusts in the inclined channel, the ratio of the distance between the lower boundary (\equiv MCTZ) to the model thrust at the vent and that between the model thrust and the upper boundary (\equiv STDS_U) were within the range of 1:0.25 to 1:1.57 (Fig. 13; see the last column in Table 2 for individual results). On the other hand, the ratio of distance between the MCT_L to the OOST and that between the OOST and the STDS_U in the natural prototype are within the range of 1:0.25 to 1:1.57 (see Fig. 6), reasonably close to those measured in the models.

This thrust in the models bear the following similarities with the OOST in the HHSZ. (1) The activities of both were recorded at the surface long after the initiation of channel flow. (2) The out-of sequence thrusting initiated at depth along with the ongoing ductile top-to-N/NE shear in the STDS_U. In turn, the OOST will be carried up at the

surface later than the initiation of the top-to-N/NE shear in the STDS_U, as happened in central Nepal at Kalopani (Vannay and Hodges 1996; Godin et al. 2001). (3) They developed inside the regime of top-to-SW compressional ductile shear. (4) The ratios of distance between the MCT_L to the OOST and that between the OOST and the STDS_U are 1:0.25 to 1:1.57 in the models and 1:0.19 to 1:1.15 in the natural prototype. Thus, values in the models and the natural prototype overlap.

Carosi et al. (2010) considered that Carosi et al.'s (2007) OOST at Toijem accommodated shortening produced by the India-Asia collision. A number of hypotheses have been suggested to explain the genesis of the OOST. These are (i) a disparity in erosion rates triggered mainly by more intense rainfall in the hanging wall of the OOST around the Marsyandi valley in Nepal (Fig. 14a; e.g. Wobus et al. 2003; Hodges et al. 2004; Wobus et al. 2005)—a process efficiently dissipated the excessive gravitational potential energy of the Tibetan plateau (Hodges et al. 2004). It is generally accepted that an OOST can form in an orogenic disequilibrium caused by relocation of rock mass by widespread erosion (review by Graveleau and Dominguez 2008). (ii) The channel flow was restricted to the upper part of the HHSZ, and the lower boundary of extrusion defined by the OOST (Fig. 14b, from Hollister and Grujic 2006). The granitic melt at depth led to this thrusting (Swapp and Hollister 1991—as referred in Grujic et al. 2002), possibly by rheological softening. (iii) At Toijem, the OOST of Carosi et al. (2007) formed as a result of extrusion at different rates across a major lithological discontinuity between gneiss in the south and marble in the north (Fig. 14c, from Carosi et al. 2007). The same reasoning may be applied to the OOST at Kalopani, where it is defined as tectonic imbrication between calc-silicate gneisses and orthogneisses (Vannay and Hodges 1996). The same applies to the Marsyandi valley where the OOST separates paragneisses of Formation-I and calc-silicate mineral bearing gneisses of Formation II (Garzanti et al. 2007). However, this hypothesis cannot apply to sectors where an OOST has been inferred without any lithological discontinuity such as in the Bhutan Himalaya (Tobgay and Hurtado 2004; Tobgay 2005). (iv) Duplexing in the Lesser Himalaya folded the MCT/STDS_U system resulted in an out-of-sequence thrusting at Kakhtang (Robinson et al. 2003; McQuarrie et al. 2008).

Our models suggest the following. (1) The OOST was formed by PDMS flowing beyond the corner joining the HHSZ and the sub-horizontal feeder channel and does not extend up-flow within the horizontal channel. (2) Since the model OOST spontaneously appeared in PDMS with its essentially constant viscosity, the prevailing tendency to link the genesis of the OOST with rheological variations within in the HHSZ (Carosi et al. 2007) is unwarranted. For

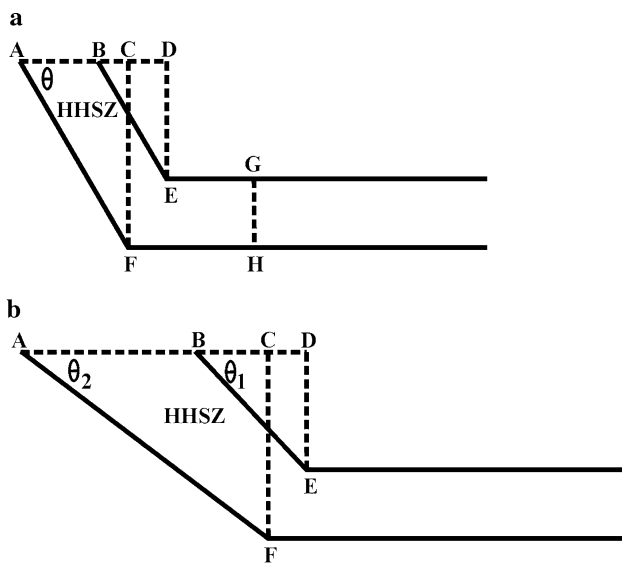


Fig. 15 **a** The Higher Himalayan Shear Zone (HHSZ) with parallel inclined boundaries AF and BE is considered. Angle FAB = angle EBD = dip of AF and BE = θ , say. Now $AF = CF \operatorname{Cosec}\theta$, and $BE = DE \operatorname{Cosec}\theta$. Therefore, $AF - BE = (CF - DE) \operatorname{Cosec}\theta = GH \operatorname{Cosec}\theta$. For $\theta = 30^\circ$; $GH = 15$ to 50 km; $(AF - BE) = 30$ to 110 km. Assuming 1 kb km^{-1} as the pressure gradient (pressure difference divided by the length of flow) near the boundary BE, the pressure gradient value near the boundary AF calculates as 0.033 to 0.009 kb km^{-1} . **b** The Higher Himalayan Shear Zone (HHSZ) with diverging-upward inclined boundaries AF and BE is considered with angles EBD as θ_1 and FAB as θ_2 . Now, $BE = DE \operatorname{Cosec}\theta_1$ and $AF = CF \operatorname{Cosec}\theta_2$. Therefore, $AF - BE = CF \operatorname{Cosec}\theta_2 - DE \operatorname{Cosec}\theta_1$. For $\theta_1 = 60^\circ$, $\theta_2 = 30^\circ$, $GH = 15$ to 50 km, $DE = 35$ km, i.e. $CF = DE + GH = 50$ to 85 km, $(AF - BE)$ is obtained as 59.58 to 129.58 km. Assuming 1 kb km^{-1} as the pressure gradient (pressure difference divided by the length of flow) near the boundary BE, the pressure gradient near the boundary AF calculates as 0.02 – 0.008 kb km^{-1}

the same reason, the buoyant effect of the less dense granitic melt now crystallized and usually confined to the hanging wall of the OOST (Grujic et al. 2002) is also unlikely to be linked with the genesis of the OOST. We emphasize that we do not try to disprove that a rheological variation exists in the prototype HHSZ. Instead, our approach has been to claim that we can successfully simulate an OOST even using a single rheology. Therefore, multiple rheologies cannot play a crucial role in the genesis of the OOST.

Our experiments using the channel flow box enabled us to simulate deformations of only the HHSZ. As the north Himalayan antiforms/gneissic domes occur in the Tethyan Sedimentary Zone outside and north to the HHSZ, they were not simulated in our analogue models. This renders any genetic relation between those antiforms/domes with the OOST (Grujic et al. 2002) unresolved but probably implausible. Further, since our models generated OOSTs without any erosion, invoking erosional—or climatic effects in the genesis of the OOST (review by Whipple

2009) appears to be unnecessary. Therefore, a higher rate of erosion in the hanging-wall side of the OOST could be one of the components, but does not look like a controlling factor for differential extrusion of the HHSZ.

A probable explanation for the disparity in extrusion rates across the inclined channel that gave rise to the model OOST is as follows. Given a particular pressure imparted by the moving piston at any instant, the length of the upper boundary of the inclined channel is less than that of the lower boundary. For example, for the HHSZ with parallel boundaries (Fig. 15a) dipping 30° and the thickness of the horizontal channel ranging between the optimum limit of 15 – 50 km (Fig. 6 of Hauck et al. 1998; Fig. 3 of Jamieson et al. 2006), the upper boundary of the inclined channel could be 30 to 110 km shorter than the lower boundary. Take 1 kb km^{-1} as the representative value of natural pressure gradient (Vannay and Grasemann 2001) along the upper boundary of the HHSZ. This leads to a pressure gradient along its lower boundary of 0.033 to 0.009 kb km^{-1} , i.e. 100 – $1,000$ times less. Assuming a diverging-upward geometry of the HHSZ (Fig. 15b) with the lower boundary dipping at 30° and the upper boundary at 60° , and the depth of the upper boundary of the horizontal channel being 35 km (Hauck et al. 1998; Vannay and Grasemann 2001; Yin 2006), increases the pressure gradient likely along the upper boundary to between 0.02 and 0.008 kb km^{-1} , of the same order as that of an inclined channel with parallel boundaries. Thus, a higher pressure gradient near the upper boundary would have driven the PDMS much faster than that along the lower boundary. The discrepancy in extrusion rate across the OOST arises simply due to channel flow having been around a corner. Even if the junction joining the horizontal to the inclined channel were curved in the prototype, the disparity in the pressure gradient near the top and bottom boundaries would remain of the same order.

The channel flow that gave rise to the OOST in the HHSZ is inferred to be a part of a master channel flow, along which the whole of the HHSZ extruded at varying rates. This conclusion is contrary to the extrusion model of Hollister and Grujic (2006). These authors portrayed an independent spatially and temporally separate pulse of channel flow leading to extrusion of the HHSZ (Fig. 14b). This pulse was confined to the northern side of the HHSZ with the OOST defining its southern boundary. Hollister and Grujic (2006) considered this confined channel flow was active during the 12 – 10 Ma when the southern part of the HHSZ did not extrude.

Morley (1988) proposed four tectonic scenarios that account for the genesis of the OOST. These are (i) the Coulomb wedge model, (ii) the deformation sequence in the overriding continental plate, (iii) local obstacles to thrust propagation, and (iv) synchronous thrusting. In

addition, as discussed earlier, four other possible mechanisms for the OOST have been described in the context of the HHSZ by Swapp and Hollister (1991), Grujic et al. (2002), Wobus et al. (2005), Hollister and Grujic (2006), Carosi et al. (2007) and McQuarrie et al. (2008). Our model proposes yet another explanation for the genesis of the OOST.

The prototype OOST displays significant variations in timing, location, thickness and displacement in space. While the OOST is inferred as a ‘surface breaking thrust’ at all other known locations, a blind thrust has been speculated beneath the Bhutan Himalaya (Tobgay and Hurtado 2004; Tobgay 2005). Our analogue models, on the other hand, have been simplistic representations of the natural extrusion of the HHSZ and cannot explain those second order tectonic details. We appreciate that the most crucial parameters that guide the extrusion of the HHSZ are (i) the shape and size of the shear zone—viz. its thickness and dip of its boundaries; (ii) The viscosity of the HHSZ rocks, and (iii) the pressure gradient driving the channel flow or the Jeffery-Hamel flow (Mukherjee and Koyi 2010a). Considering Mukherjee and Koyi’s (2010a, b) review, maximum variations in these parameters in the HHSZ are 30° in dip of the shear zone boundaries, 70 km in thickness of the shear zone, $\sim 1.9 \text{ kbar km}^{-1}$ in the pressure gradient and a 10^{14} Pa s difference between the viscosity of partially molten mid-crustal rocks and a granitic melt. Such enormous variations in parameters over hundreds of km along the length of the HHSZ might account for the spatial and kinematic variability of its OOST. Further, the following possible variations could also secondarily affect the extrusion. (1) The boundaries of the deep HHSZ could have varied from parallel to tapering. (2) The presence of a number of lithologies—mainly schists and gneisses—in the same section of the HHSZ mean that the shear zone could be considered as a number of fluids with different effective viscosities. (3) Partially molten rocks would become more sluggish as they approached the surface and cooled. (4) The rate of erosion controlled mainly by the monsoon precipitation on the HHSZ varied by section. One of the manifestations of variability in some of the extrusion parameters is demonstrated by an increase in the rate of exhumation of the HHSZ from $\sim 1.5 \text{ mm year}^{-1}$ during 2–0.6 Ma to $\sim 2\text{--}5 \text{ mm year}^{-1}$ from ~ 0.8 till the present in central Nepal (Blythe et al. 2007). Similarly the extrusion rate fell from $\sim 15 \text{ mm year}^{-1}$ up to a depth of 15 km to 2 mm year^{-1} up to $\sim 5 \text{ km}$ in the Sikkim Himalaya (Ganguly et al. 2000).

Further, Leech (2008) showed that the channel flow concomitant to that within the HHSZ also extruded the Leo Pargil Dome north of the HHSZ at around 18 Ma. In addition, Kirstein et al. (2006) demonstrated that channel flow was also active in the Ladakh Batholith, further north

of the Leo Pargil Dome, contemporaneously with extrusion in the HHSZ. Kirstein et al. (2006) concluded that extrusion due to channel flow did not lead to simple southward propagation of deformation in the Himalaya. Our analogue models showed that extrusion created by channel flow from a horizontal channel flat into an inclined HHSZ ramp intrinsically led to an OOST that focused deformation in the northern part of the HHSZ in the late phase of extrusion. Therefore, our study is a further corroboration of Kirstein et al.’s (2006) surmise that no simple relation existed between channel flow and spatial and temporal variation of deformation in the Himalaya. Finally, even if the modelled MCT and the STDS had been lubricated, a parabolic profile would still have developed and our qualitative results would stand. In HHSZ sections where the OOST has not yet been reported at the surface, the OOST might still be present but as a blind fault. Where the OOST appears in the future may be marked by appropriate seismicity within the HHSZ.

Conclusions

An out-of-sequence thrust (OOST) was active within the Higher Himalayan Shear Zone (HHSZ) from 22 Ma until the Holocene. It usually postdated the beginning of HHSZ extrusion pushed by channel flow. The OOST is a 50 m- to 6-km-thick north-east dipping shear zone of high strain rate, with a throw of 1.4–20 km and with migmatites dominant in the hanging wall. The ratio of distance between the Main Central Thrust-Lower (MCT_L) to the OOST and that between the OOST and the South Tibetan Detachment System-Upper (STDS_U) is between 1:0.25 to 1:1.57.

In analogue models, polydimethylsiloxane (PDMS) was pushed at constant rates through a horizontal channel so that it extruded through a linked inclined channel with parallel and diverging-upward geometries. The inclined channel—the model HHSZ—developed a zone of top-to-N/NE shear towards the upper boundary equivalent to the STDS_U. Similarly, a zone of compressional shear developed towards its lower boundary without any simultaneous development of the South Tibetan Detachment System-Lower (STDS_L). This indicates that top-to-N/NE shear in the STDS_L was produced in a spatially and temporally separate and independent pulse of channel flow that occupied the southern part of the inclined HHSZ. Secondly, the PDMS originally inside the horizontal channel extruded preferentially through the upper part of the inclined channel. The lower boundary of the faster-flowing fluid layer defined an out-of-sequence thrust (OOST). The OOST originated at the corner joining the horizontal and inclined channels. Continued extrusion carried the model

OOST to the vent where the ratio of the distances between it and the lower boundary of the inclined channel to that between it and the upper boundary of the inclined channel is within 1:0.25 to 1:1.57. Since the models were run with a single deformable material and without any erosion at the vent, neither internal rheological contrast nor climatic factor seems to be the necessary explanations for the genesis of the OOST. Instead, the OOST is intrinsically linked to channel flow past a corner that involved a pressure gradient near the $STDS_U$ 100 to 1000 times higher than that near the MCT_L . The models also imply that such OOSTs may also form in other orogenies if the channel flow changes its flow direction significantly such as in the Grenville province (figs. 10a, b and 11a–c of Rivers 2009).

An enormous variation in timing, level within the HHSZ, and thickness and displacement of the OOST along the Himalayan trend can be attributed to variation in shape, size and rheology of the HHSZ, differences in the pressure gradient and the rate of erosion. The models, however, generated a temporally increasing pressure gradient in the horizontal channel. This cannot be correlated with the real situation of the partially molten mid-crustal rocks of the Tibetan Plateau. Extrusion in the Himalaya due to channel flow did not result in southward propagation of deformation.

Acknowledgments SM acknowledges Swedish Institute's (Stockholm) 'Guest Scholarship' that enabled the authors to perform analogue models together at Hans Ramberg Tectonic Laboratory, Uppsala University during 2005–2006. SM finalized the manuscript with IIT Bombay's flexible *Seed Grant: Spons/GS/SM-1/2009*. HAK was supported by the Swedish Research Council. We thank S. Karlsson (Uppsala University) for constructing and adapting the 'channel flow box' (Fig. 8) to our design. Discussions with R. Govindarajan (Jawaharlal Nehru Center for Advanced Scientific Research) on channel flow—especially on establishing the dynamic similarity between the model and the natural prototype—were beneficial. SM thanks his students A. Ghosh for raising several doubts and M. Bose for improving a number of figures. S. Bhattacharyya (Alabama University) and A. Ghatak (Rochester University) constantly updated SM on Himalayan geological literatures. Numerous clarifications sought by L. Godin (Queen's University), B.C. Burchfiel (MIT) and an anonymous reviewer led us to strengthen our arguments, and to shuffle and shorten the manuscript. W.C. Dullo is thanked for his efficient editorial handling despite suffering a road accident. The present attempts of analogue models have been referred by Mandal (2008).

Appendix

The Plane Poiseuille flow of velocity profile in zone 2 is given by

$$U = -0.5 \mu^{-1} (dP/dx) (y_0^2 - y^2) \quad \text{Pai (1956)} \quad (1)$$

where U : velocity of the fluid; $2y_0$: thickness of the channel; μ : dynamic viscosity of the fluid; and dP/dx :

pressure gradient in the X-direction. The X-axis is considered equidistant from the horizontal channel boundaries. The vertex of the parabolic profile is $[0.5 \mu^{-1} y_0^2 (dP/dx), 0]$. The parameters $2y_0$ and μ being known, measuring the coordinate of the vertex of the parabola from photographs taken at intervals and plotted against time allows constraint of the temporal increase in the pressure gradient in the horizontal channel (Fig. 9). These plots are fitted with the straight line equation

$$(dP/dx) = (at + b) \quad (2)$$

where (dP/dx) is in dyne cm^{-3} and ' t ' is in seconds. The correlation coefficients in all the cases are >0.9 . The set of 'a' and 'b' values in Eq. 2 for different experiments are presented in the thirteenth and fourteenth columns in Table 2.

The Reynolds Number is defined as

$$R_e = \rho v y_0 \mu^{-1} \quad (3)$$

here ρ : density, μ : dynamic viscosity of the fluid, y_0 : half the width of the channel, and v : velocity of flow. In the natural prototype of the HHSZ, taking crustal density $\rho = 2.7 \text{ gm cm}^{-3}$, viscosity of partially molten rocks $\mu = 10^{19} \text{ Pa s}$ (as taken by Jamieson et al. 2004), $v \sim 3.3 \text{ mm year}^{-1}$ (extrusion rate of the Zaskar Shear Zone, a continuation of the $STDS_U$, as per Yin 2006), R_e comes out in the order of 10^{-21} . On the other hand, in analogue models, for PDMS, taking $\rho = 0.95 \text{ gm cm}^{-3}$, $\mu = 10^5 \text{ Pa s}$ (Talbot and Aftabi 2004 and references therein), the slowest velocity of extrusion attained $v = 3 \text{ mm per 10 min}$, and half the width of the model HHSZ ($y_0 = 1.25 \text{ cm}$ in few experiments, R_e in the order of 10^{-14} is obtained. Both these values are sufficiently small so that inertia can be neglected.

References

- Acharya SK, Ray KK (1977) Geology of the Darjeeling-Sikkim Himalaya. In: Guide to Excursion No. 4 Fourth International Gondwana Symposium, India, report. 25 pp, Calcutta, India
- Ashish, Padhi A, Rai SS et al (2009) Seismological evidence for shallow crustal melt beneath the Garhwal High Himalaya, India: implications for the Himalayan channel flow. *Geophys J Int* 177:1111–1120. doi:10.1111/j.1365-246X.2009.04112.x
- Beaumont C, Jamieson RA, Nguyen MH et al (2001) Himalayan tectonics explained by extrusion of a low-viscosity crustal channel coupled to focused surface denudation. *Nature* 414:738–742. doi:10.1038/414738a
- Beaumont C, Jamieson RA, Nguyen MH et al (2004) Crustal channel flows: 1. Numerical models with applications to the tectonics of the Himalayan-Tibetan orogen. *J Geophys Res* 109:1–29. doi:10.1029/2003JB002809
- Blythe AE, Burbank DW, Carter A (2007) Plio-Quaternary exhumation history of the central Nepalese Himalaya: 1. Apatite and

- zircon fission track and apatite [U-Th]/He analyses. *Tectonics* 26:TC3002. doi:10.1029/2006TC001990
- Burbank DW (2005) Earth science: cracking the Himalaya. *Nature* 434:963–964. doi:10.1038/434963a; <http://www.nature.com/nature/journal/v434/n7036/full/434963a.html>
- Burbank DW, Blythe AE, Putkonen J et al (2003) Decoupling of erosion and precipitation in the Himalayas. *Nature* 426:652–654. doi:10.1038/nature02187; http://projects.crustal.ucsb.edu/nepal/publications/Burbank_etal2003.pdf
- Burchfiel BC, Chen Z, Hodges KV et al (1992) The South Tibetan detachment system, Himalayan orogen: extension contemporaneous with and parallel to shortening in a collisional mountain belt. *Geol Soc Am Spec Pap* 269:1–41
- Caldwell WB, Klempner SL, Rai SS et al (2009) Partial melt in the upper-middle crust of the northwestern Himalaya revealed by Rayleigh wave dispersion. *Tectonophysics* 477:58–65. doi:10.1016/j.tecto.2009.01.013
- Carosi R, Montomoli C, Visonà D (2007) A structural transect in the lower Dolpo: insights in the tectonic evolution of Western Nepal. *J Asian Earth Sci* 29:407–423. doi:10.1016/j.jseae.2006.05.001
- Carosi R, Montomoli C, Rubatto D et al (2010) Late oligocene high temperature shear zones in the core of the Higher Himalayan Crystallines (Lower Dolpo, western Nepal). *Tectonics* 29:TC4029. doi:10.1029/2008TC002400
- Catlos EJ, Harrison TM, Kohn MJ et al (2001) Geochronologic and thermobarometric constraints on the evolution of the Main Central Thrust, central Nepal Himalaya. *J Geophys Res* 106:16177–16204. doi:10.1029/2000JB900375
- Chambers JA, Argles TW, Horstwood MSA et al (2008) Tectonic implications of Palaeoproterozoic anatexis and Late Miocene metamorphism in the Lesser Himalayan Sequence, Sutlej valley, NW India. *J Geol Soc Lond* 165:725–737. doi:10.1144/0016-76492007/090
- Chambers J, Parrish R, Argles T et al (2011) A short duration pulse of ductile normal shear on the outer South Tibetan Detachment in Bhutan: alternating channel flow and critical taper mechanics of the eastern Himalaya. *Tectonics* (in press)
- Coleman ME (1998) U-Pb constraints on oligocene miocene deformation and anatexis within the central Himalaya, Marsiyandi valley, Nepal. *Am J Sci* 298:553–571
- Depietro JA, Pogue KR (2004) Tectonostratigraphic subdivision of the Himalaya—a view from the west. *Tectonics* 23:TC 5001. doi:10.1029/2003TC001554
- Dewey L (2008) Continental lower-crustal flow: channel flow and laminar flow. *Earth Sci Frontiers* 15:130–139. doi:10.1016/S1872-5791(08)60065-2
- Dèzes PJ, Vannay JC, Steck A et al (1999) Synorogenic extension: quantitative constraints on the age and displacement of the Zaskar shear Zone. *Geol Soc Am Bull* 111:364–374. doi:10.1130/0016-7606(1999)111<0364:SEQCOT>2.3.CO;2
- Exner U (2005) Analog modelling of flanking structures. Unpublished Ph.D. thesis, ETH, pp 65–78
- Ganguly J, Dasgupta S, Cheng W et al (2000) Exhumation history of a section of the Sikkim Himalayas, India: records in the metamorphic mineral equilibria and compositional zoning of garnet. *Earth Planet Sci Lett* 183:471–486. doi:10.1016/S0012-821X(00)00280-6
- Garzanti W, Vezzoli G, Andò S et al (2007) Quantifying sand provenance and erosion (Marsiyandi River, Nepal Himalaya). *Earth Planet Sci Lett* 258:500–515. doi:10.1016/j.epsl.2007.04.010
- Godin L, Parrish RR, Brown RL et al (2001) Crustal thickening leading to exhumation of the Himalayan metamorphic core of central Nepal; insight from U-Pb geochronology and ⁴⁰Ar/³⁹Ar thermochronology. *Tectonics* 20:729–747
- Godin L, Grujic D, Law RD et al (2006) Channel flow, extrusion and extrusion in continental collision zones: an introduction. In: Law RD, Searle MP (eds) Channel flow, extrusion and extrusion in continental collision zones. *Geol Soc Lond Spec Publ* 268:1–23. doi:10.1144/GSL.SP.2006.268.01.01
- Godin L, Yakymchuk C, Harris LB (2011) Himalayan hinterland-verging superstructure folds related to foreland-directed infrastructure ductile flow: insights from centrifuge analogue modeling. *J Struct Geol* 33:329–342. doi:10.1016/j.jsg.2010.09.005
- Goscombe B, Gray D, Hand M (2006) Crustal architecture of the Himalayan metamorphic front in eastern Nepal. *Gond Res* 10:232–255. doi:10.1016/j.gr.2006.05.003
- Grasemann B, Edwards MA, Wiesmayr G (2006) Kinematic dilatancy effects on orogenic extrusion. In: Law RD, Searle MP, Godin L (eds) Channel flow, ductile extrusion and extrusion in continental collision zones. *Geol Soc Lond Spec Publ* 268:183–199. doi:10.1144/GSL.SP.2006.268.01.08
- Graveleau F, Dominguez S (2008) Analogue modelling of the interaction between tectonics, erosion and sedimentation in foreland thrust belts. *C R Geosci* 340:324–333. doi:10.1016/j.crte.2008.01.005
- Grujic D (2006) Channel flow and continental collision tectonics: an overview. In: Law RD, Searle MP (eds) Channel flow, extrusion and exhumation in continental collision zones. *Geol Soc Lond Spec Publ* 268:25–37. doi:10.1144/GSL.SP.2006.268.01.02
- Grujic D, Casey M, Davidson C (1996) Ductile extrusion of the Higher Himalayan Crystalline in Bhutan: evidence from quartz microfabrics. *Tectonophysics* 260:21–43. doi:10.1016/0040-1951(96)00074-1
- Grujic D, Hollister LS, Parrish RR (2002) Himalayan metamorphic sequence as an orogenic channel: insight from Bhutan. *Earth Planet Sci Lett* 198:177–191. doi:10.1016/S0012-821X(02)00482-X
- Harris N (2007) Channel flow and the Himalayan-Tibetan orogen: a critical review. *J Geol Soc London* 164:511–523. doi:10.1144/0016-76492006-133
- Harrison TM (2006) Did the Himalayan Crystallines extrude partially molten from beneath the Tibetan Plateau? In: Law RD, Searle MP, Godin L (eds) Channel flow, ductile extrusion and exhumation in continental collision zones. *Geol Soc Lond Spec Publ* 268:237–254
- Harrison TM, Ryerson FJ, Le Fort P et al (1997) A Late Miocene-Pliocene origin for the Central Himalayan inverted metamorphism. *Earth Planet Sci Lett* 146:E1–E7. doi:10.1016/S0012-821X(96)00215-4
- Hauck ML, Nelson KD, Brown LD et al (1998) Crustal structure of the Himalayan orogen at 90° east longitude from project INDEPTH deep seismic reflection profiles. *Tectonics* 17:481–500. doi:10.1029/98TC01314
- Hodges KV (2006) A synthesis of the channel flow-extrusion hypothesis as developed for the Himalayan-Tibetan orogenic system. In: Law RD, Searle MP (eds) Channel flow, extrusion and exhumation in continental collision zones. *Geol Soc Lond Spec Publ* 268:71–90. doi:10.1144/GSL.SP.2006.268.01.04
- Hodges KV, Parrish RR, Searle MP (1996) Tectonic evolution of the central Annapurna Range, Nepalese Himalayas. *Tectonics* 15:1264–1291
- Hodges KV, Wobus C, Ruhl K et al (2004) Quaternary deformation, river steepening, and heavy precipitation at the front of the Higher Himalayan ranges. *Earth Planet Sci Lett* 220:379–389. doi:10.1016/S0012-821X(04)00063-9
- Hollister LS, Grujic D (2006) Himalaya Tiber Plateau. Pulsed channel flow in Bhutan. In: Law RD, Searle MP, Godin L (eds) Channel flow, ductile extrusion and extrusion in continental collision zones. *Geol Soc Lond Spec Publ* 268:415–423. doi:10.1144/GSL.SP.2006.268.01.19

- Imayama T, Takeshita T, Arita K (2010) Metamorphic P–T profile and P–T path discontinuity across the far-eastern Nepal Himalaya: investigation of channel flow models. *J Meta Geol* 28:527–549. doi:[10.1111/j.1525-1314.2010.00879.x](https://doi.org/10.1111/j.1525-1314.2010.00879.x)
- Jain AK, Anand A (1988) Deformational and strain patterns of an intracrustal ductile shear zone- an example from the Higher Garhwal Himalaya. *J Struct Geol* 10:717–734. doi:[10.1016/0191-8141\(88\)90079-X](https://doi.org/10.1016/0191-8141(88)90079-X)
- Jain AK, Kumar D, Singh S et al (2000) Timing, quantification and tectonic modelling of pliocene-quatertiary movements in the NW Himalaya: evidences from fission track dating. *Earth Planet Sci Lett* 179:437–451. doi:[10.1016/S0012-821X\(00\)00133-3](https://doi.org/10.1016/S0012-821X(00)00133-3)
- Jain AK, Singh S, Manickavasagam RM (2002) Himalayan collisional tectonics. *Gond Res Gp Mem No. 7*. Field Science, Hashimoto
- Jain AK, Mukherjee S, Singh S (2005) Great Himalayan orogenic channel: its structure and tectonic patterns. Abstract number: 58-SE-A1226. *Solid Earth*. Asia Oceania Geosciences Society. 2nd Annual General Meeting 20-24 June 2005, Singapore. <http://www.asiaoceania.org/abstract/se/58-SE-A1226.pdf>
- Jamieson RA, Beaumont C, Medvedev S et al (2004) Crustal channel flows: 2. Numerical models with implications for metamorphism in the Himalayan–Tibetan Orogen. *J Geophys Res* 109:B06407. doi:[10.1029/2003JB002811](https://doi.org/10.1029/2003JB002811)
- Jamieson RA, Beaumont C, Nguyen P et al (2006) Provenance of the greater himalayan sequence and associated rocks: predictions of channel flow models. In: Law RD, Searle MP (eds) *Channel flow, extrusion and extrusion in continental collision zones*. Geological Soc Lond Spec Publ 268:165–182. doi:[10.1144/GSL.SP.2006.268.01.07](https://doi.org/10.1144/GSL.SP.2006.268.01.07)
- Jessup MJ, Law RD, Searle MP et al (2006) Structural evolution and vorticity of flow during extrusion and exhumation of the Greater Himalayan Slab, Mount Everest Massif, Tibet/Nepal: implications for orogen-scale flow partitioning, vol 268. Geological Society of London, Special Publication, pp 379–413. doi:[10.1144/GSL.SP.2006.268.01.18](https://doi.org/10.1144/GSL.SP.2006.268.01.18)
- Kirstein LA, Sinclair H, Stuart FM et al (2006) Rapid early Miocene exhumation of the Ladakh batholith, western Himalaya. *Geol Soc Am Bull* 117:1049–1052
- Kohn MJ (2008) P–T–t data from central Nepal support critical taper and reduplicate large-scale channel flow of the Greater Himalayan sequence. *Geol Soc Am Bull* 120:259–273. doi:[10.1130/B26252.1](https://doi.org/10.1130/B26252.1)
- Koyi H (1991) Mushroom diapirs penetrating into high viscous overburden. *Geology* 19:1229–1232
- Koyi H (1997) Analogue modelling: from a qualitative to a quantitative technique, a historical outline. *J Petrol Geol* 20:223–238
- Langille J, Lee J, Hacker B et al (2010) Middle crustal ductile deformation patterns in southern Tibet: insights from vorticity studies in Mabja Dome. *J Struct Geol* 32:70–85. doi:[10.1016/j.jsg.2009.08.009](https://doi.org/10.1016/j.jsg.2009.08.009)
- Larson J, Godin L (2009) Kinematics of the Greater Himalayan sequence, Dhaulagiri Himal: implications for the structural framework of the central Nepal Himalaya. *J Geol Soc Lond* 166:25–43
- Law R, Searle MP, Simpson RL (2004) Strain, deformation temperatures and vorticity of flow at the top of the Greater Himalayan Slab, Everest Massif, Tibet. *J Geol Soc Lond* 161:305–320. doi:[10.1144/0016-764903-047](https://doi.org/10.1144/0016-764903-047)
- LeCureux F, Burnett J (1975) Graphical methods used in the numerical solution of Jeffery–Hamel flow at fixed flow rates. *Comput Graph* 1:233–238. doi:[10.1016/0097-8493\(75\)90013-8](https://doi.org/10.1016/0097-8493(75)90013-8)
- Lee J, Whitehouse MJ (2007) Onset of midcrustal extensional flow in southern Tibet: evidence from U/Pb zircon ages. *Geology* 35:45–48
- Leech ML (2008) Does the Karakoram fault interrupt mid-crustal channel flow in the western Himalaya? *Earth Planet Sci Lett* 276:314–322. doi:[10.1016/j.epsl.2008.10.006](https://doi.org/10.1016/j.epsl.2008.10.006)
- Leloup PH, Mahè G, Arnaud N et al (2010) The South Tibet detachment shear zone in the Dinggye area Time constraints on extrusion models of the Himalayas. *Earth Planet Sci Lett* 292:1–16
- Mandal N (2008) Glimpse of experimental structural geology in India. In: Singhvi A, Bhattacharya A, Guha S (eds) *Glimpse of geoscience research in India*. The Indian Report to IUGS 2004–2008. pp 153–157. URL:<http://www.iypeinsa.org/updates-09/art-30.pdf>
- Martin A, DeCelles P, Gehrels GE et al (2005) Isotopic and structural constraints on the location of the Main Central thrust in the Annapurna Range, central Nepal Himalaya. *Geol Soc Am Bull* 117:926–944. doi:[10.1130/B25646.1](https://doi.org/10.1130/B25646.1)
- Massey BS (1975) *Mechanics of fluids*, 3rd edn edn. Van Nostrand Reinhold Company, New York, p 145
- McQuarrie N, Robinson D, Long S et al (2008) Preliminary stratigraphic and structural architecture of Bhutan: implications for the along strike architecture of the Himalayan system. *Earth Planet Sci Lett* 272:105–117. doi:[10.1016/j.epsl.2008.04.030](https://doi.org/10.1016/j.epsl.2008.04.030)
- Morley CK (1988) Out-of-sequence thrusts. *Tectonics* 7:539–561
- Mukherjee S (2005) Channel flow, ductile extrusion and exhumation of lower-middle crust in continental collision zones. *Curr Sci* 89:435–436. <http://www.iisc.ernet.in/currensci/aug102005/435.pdf>
- Mukherjee S (2007) Geodynamics, deformation and mathematical analysis of metamorphic belts of the NW Himalaya. Unpublished Ph.D. thesis, Indian Institute of Technology, Roorkee, pp 1–267
- Mukherjee S (2010a) Structures at meso and micro-scales in the Sutlej section of the Higher Himalayan Shear Zone in Himalaya. *e-Terra* 7(1):1–27. <http://metododirecto.pt/ojs/index.php/e-terra/article/view/33/21>
- Mukherjee S (2010b) Microstructures of the Zaskar Shear Zone. *Earth Sci India* 3(1):9–27. <http://www.earthscienceindia.info/PDF/Mukherjee.pdf>
- Mukherjee S (2010c) Estimating the viscosity of rock bodies—a comparison between the Hormuz and the Namakdan salt diapirs in the Persian Gulf, and the Tso Morari Gneiss dome in the Himalaya. *J Indian Geophys Union*, (Submitted)
- Mukherjee S, Jain AK (2004) Numerical modeling, deformation and exhumation patterns in the Higher Himalayan channel, Sutlej Valley, Himachal Pradesh, India. Abstract. In: *Channel flow, ductile extrusion and exhumation of lower-mid crust in continental collision zones*. Geological Society of London, Burlington House, 6–7 December
- Mukherjee S, Koyi HA (2010a) Higher Himalayan Shear Zone, Sutlej section- structural geology and extrusion mechanism by various combinations of simple shear, pure shear and channel flow in shifting modes. *Int J Earth Sci* 99:1267–1303. doi:[10.1007/s00531-009-0459-8](https://doi.org/10.1007/s00531-009-0459-8)
- Mukherjee S, Koyi HA (2010b) Higher Himalayan Shear Zone, Zaskar Indian Himalaya—microstructural studies and extrusion mechanism by a combination of simple shear and channel flow. *Int J Earth Sci* 99:1083–1110. doi:[10.1007/s00531-009-0447-z](https://doi.org/10.1007/s00531-009-0447-z)
- Mukherjee S, Mulchrone K (2011) Estimating the viscosity of the Tso Morari Gneiss dome, western Indian Himalaya. *Int J Earth Sci* (submitted)
- Mukherjee S, Koyi HA, Talbot CJ (2009) Out-of-sequence thrust in the Higher Himalaya—a review and possible genesis, vol 11. EGU2009-13783. European Geosciences Union General Assembly. *Geophys Res Abs*. Vienna, Austria, 19–24 April. <http://meetingorganizer.copernicus.org/EGU2009/EGU2009-13783.pdf>

- Mukherjee S, Talbot CJ, Koyi HA (2010) Viscosity estimates of salt in the Hormuz and Namakdan salt diapirs, Persian Gulf. *Geol Mag* 147:497–507
- Mukherjee S, Jain L, Samajdar I et al (2011) In-grain variation of strain in the Tso Morari Gneiss dome (Indian western Himalaya) revealed by EBSD studies supports its channel flow extrusion (submitted)
- Owen LA (2010) Landscape development of the Himalayan-Tibet orogen: a review. In: Kusky TM, Zhai M-G, Xiao W (eds) *The evolving continents: understanding processes of continental growth*. *Geol Soc Lond Spec Pub* 338:389–407
- Pai S-I (1956) *Viscous flow theory I—laminar flow*. Van Nostrand Company Inc, D. New Jersey, p 51
- Paul A, Bhakuni SS, Pant CC et al (2010) Microseismicity in central part of the Inner Kuamaun Lesser Himalaya: implication to active seismotectonics. *Him Geol* 31:107–115
- Ramberg H (1981) *Gravity, deformation and the Earth's crust in theory experiments and geological applications*, 2nd edn. Academic Press, London, pp 5–6
- Rivers T (2009) The Grenville province as a large hot long-duration collisional orogen—insights from the spatial and thermal evolution of its orogenic fronts. In: Murphy JB, Keppie JD, Hynes AJ (eds) *Ancient orogens and modern analogues*. *Geol Soc Lond Spec Pub* 327:405–444
- Robinson DM, DeCelles PG, Garzzone CN et al (2003) Kinematic model for the main central thrust in Nepal. *Geology* 31:359–362. doi:10.1130/0091-7613(2003)031<0359:KMFTMC>2.0.CO;2
- Robinson D, DeCelles PG, Copeland P (2006) Tectonic evolution of the Himalayan thrust belt in western Nepal: Implications for channel flow models. *Geol Soc Am Bull* 118:865–885. doi:10.1130/B25911.1
- Rowe CD (2007) Comparison between three out-of-sequence thrusts from Japan and Alaska: implications for Nankai drilling targets from the rock record. *Sci Drill* 1:82–83 special edition
- Schlichting H, Gersten K (1999) *Boundary layer theory*. 8th revised enlarged edition. Springer, Berlin, pp 101–104
- Searle MP (1999) Extensional and compressional faults in the Everest-Lhotse massif, Khumbu Himalaya, Nepal. *J Geol Soc Lond* 156:227–240. doi:10.1144/gsjgs.156.2.0227
- Searle MP, Rex AJ (1989) Thermal model for the Zaskar Himalaya. *J Meta Petrol* 7:127–134
- Searle MP, Simpson RL, Law RD (2003) The structural geometry, metamorphic and magmatic evolution of the Everest massif, High Himalaya of Nepal-South Tibet. *J Geol Soc Lond* 160:345–366. doi:10.1144/0016-764902-126
- Stephenson BJ, Waters DJ, Searle MP (2000) Inverted metamorphism and the Main Central Thrust: field relations and thermobarometric constraints from the Kishtwar Window, NW Indian Himalaya. *J Meta Geol* 18:571–590. doi:10.1046/j.1525-1314.2000.00277.x
- Stüwe K (2007) *Geodynamics of the lithosphere*, 2nd edn. Springer, Berlin, p 325
- Swapp SM, Hollister LS (1991) Inverted metamorphism within the Tibetan slab of Bhutan: evidence for a tectonically transported heat source. *Can Mineral* 29:1019–1041
- Sykes JB, Reid WH (1984) *Fluid mechanics*, 2nd edn. Pergamon, Oxford, pp 76–81
- Talbot CJ, Aftabi P (2004) Geology and models of salt extrusion at Qum Kuh, central Iran. *J Geol Soc Lond* 161:321–334. doi:10.1144/0016-764903-102
- Thakur VC (1992) *Geology of Western Himalaya*. Pergamon, Oxford
- Tobgay T (2005) Unique topography of the Bhutan Himalaya: implications for active tectonics. ETD Collection for University of Texas, El Paso, Paper AAI1430972. URL: <http://digitalcommons.utep.edu/dissertations/AAI1430972>
- Tobgay T, Hurtado JM Jr (2004) Active uplift in the Bhutan Himalaya as indicated by bedrock river profiles. In: Denver annual meeting. Geological Society of America abstracts with programs, vol 36, p 505
- Vannay J-C, Grasemann B (2001) Himalayan inverted metamorphism and syn-convergence extension as a consequence of a general shear extrusion. *Geol Mag* 138:253–276. doi:10.1017/S0016756801005313
- Vannay J-C, Hodges KV (1996) Tectonomorphic evolution of the Himalayan metamorphic core between the Annapurna and Dhaulagiri, central Nepal. *J Meta Geol* 14:635–656
- Vannay JC, Grasemann B, Rahn M et al (2004) Miocene to holocene exhumation of metamorphic crustal wedge in the NW Himalaya: evidence for tectonic extrusion coupled to fluvial erosion. *Tectonics* 23(TC1014):1–24. doi:10.1029/2002TC001429
- Whipple KX (2009) The influence of climate on the tectonic evolution of mountain belts. *Nat Geosci* 2:97–104. doi:10.1038/ngeo413. URL: <http://www.ig.utexas.edu/steep/data/Whipple.2009.climate%20and%20tectonics.pdf>
- Wobus C (2005) *Geomorphic and thermochronologic signature of active tectonics in the Central Nepalese Himalaya*. Ph.D. thesis, Massachusetts Institute of Technology, pp 1–207
- Wobus CW, Hodges KV, Whipple KX (2003) Has focused denudation sustained active thrusting at the Himalayan topographic front? *Geology* 31:861–864
- Wobus C, Heimsath A, Whipple K et al (2005) Active out-of-sequence thrust faulting in the central Nepalese Himalaya. *Nature* 434:1008–1011. doi:10.1038/nature03499
- Wobus C, Whipple KX, Hodges KV et al (2006a) Tectonics of the central Nepalese Himalaya: Constraints from geomorphology, detrital $^{40}\text{Ar}/^{39}\text{Ar}$ thermochronology, and thermal modeling. *Tectonics* 25:TC4011, doi:10.1029/2005TC001935
- Wobus C, Whipple KX, Kirby E. et al (2006b) Tectonics from topography: Procedures, promise and pitfalls. In: Willett SD, Hovius N, Brandon MT, Fisher DM (eds). *Tectonics, Climate and Landscape Evolution: Geological Society of America Special Publication 398*, Penrose Conference Series, pp. 55-74. doi:10.1130/2006.2398(04)
- Wobus C, Pringle M, Whipple K et al (2008) A Late Miocene acceleration of extrusion in the Himalayan crystalline core. *Earth Planet Sci Lett* 269:1–10. doi:10.1016/j.epsl.2008.02.019
- Yin A (2006) Cenozoic tectonic evolution of the Himalayan orogen as constrained by along-strike variation of structural geometry, extrusion history, and foreland sedimentation. *Earth-Sci Rev* 76:1–131. doi:10.1016/j.earscirev.2005.05.004
- Yin A, Dubey CS, Kelty TK et al (2006) Structural evolution of the Arunachal Himalaya and implications for asymmetric development of the Himalayan orogen. *Curr Sci* 90:195-206. <http://www.ias.ac.in/currsci/jan252006/195.pdf>